

MarQSim: Reconciling Determinism and Randomness in Compiler Optimization for Quantum Simulation

XIUQI CAO, University of Pennsylvania, USA
 JUNYU ZHOU, University of Pennsylvania, USA
 YUHAO LIU, University of Pennsylvania, USA
 YUNONG SHI, AWS Quantum Technology, USA
 GUSHU LI, University of Pennsylvania, USA

Quantum simulation, fundamental in quantum algorithm design, extends far beyond its foundational roots, powering diverse quantum computing applications. However, optimizing the compilation of quantum Hamiltonian simulation poses significant challenges. Existing approaches fall short in reconciling deterministic and randomized compilation, lack appropriate intermediate representations, and struggle to guarantee correctness. Addressing these challenges, we present MarQSim, a novel compilation framework. MarQSim leverages a Markov chain-based approach, encapsulated in the Hamiltonian Term Transition Graph, adeptly reconciling deterministic and randomized compilation benefits. We rigorously prove its algorithmic efficiency and correctness criteria. Furthermore, we formulate a Min-Cost Flow model that can tune transition matrices to enforce correctness while accommodating various optimization objectives. Experimental results demonstrate MarQSim’s superiority in generating more efficient quantum circuits for simulating various quantum Hamiltonians while maintaining precision.

1 INTRODUCTION

One of the most fundamental principles in quantum algorithm design is the concept of quantum simulation, often referred to as Hamiltonian simulation. Inspired initially by Feynman’s visionary proposal for developing a quantum computer [19], this notion represents a pivotal application of quantum computing [2, 39]. Quantum simulation involves emulating quantum physical systems, a task of paramount importance that extends beyond simulation itself. Quantum algorithms have since harnessed the power of simulation to address an array of applications, such as solving linear system [25], quantum principal component analysis [40], and quantum support vector machine [54]. These algorithms necessitate the simulation of quantum systems carefully crafted to address specific computational problems. Notably, alongside digital quantum computing, the analog quantum simulation becomes a promising candidate to demonstrate quantum advantage since it provides excellent efficiency by directly mapping the simulated Hamiltonian onto the device Hamiltonian without the quantum circuit abstraction [14, 53].

The quantum simulation process is usually described by the operator $e^{i\mathcal{H}t}$ where \mathcal{H} is the Hamiltonian of the target quantum system and $t \in \mathbb{R}$ is the evolution time of the simulated system. To implement this operator on a quantum computer, a common practice is to decompose the Hamiltonian into a weighted sum of some Hamiltonian terms $\mathcal{H} = \sum_j h_j H_j$ where $h_j \in \mathbb{R}$ is the weight, and H_j is the Hamiltonian term. A typical selection of H_j is the Pauli strings due to the simple implementation of $e^{i\theta_j H_j}$ ($\theta_j \in \mathbb{R}$ is a real parameter and H_j is a Pauli string). Finally, implementing operator $e^{i\mathcal{H}t}$ is turned into combining the simulation of all these Hamiltonian terms $e^{i\theta_j H_j}$ and the compilation usually results in a very long quantum gate sequence. Even for the analog quantum simulation without the quantum circuit abstraction, decomposing and manipulating the Hamiltonian terms are still required in its Hamiltonian compilation [53].

Authors’ Contact Information: Xiuqi Cao, University of Pennsylvania, Philadelphia, USA, ; Junyu Zhou, junyuzh@seas.upenn.edu, University of Pennsylvania, Philadelphia, USA; Yuhao Liu, University of Pennsylvania, Philadelphia, USA, liuyuhao@seas.upenn.edu; Yunong Shi, AWS Quantum Technology, New York, USA; Gushu Li, University of Pennsylvania, Philadelphia, USA, gushuli@seas.upenn.edu.

Optimizing the compilation of quantum Hamiltonian simulation is imperative to harness the potential of quantum simulation fully. However, the existing compilation approaches for quantum Hamiltonian simulation are still far from optimal, and we briefly summarize three major challenges.

Seemingly Incompatible Compilation Approaches: The first challenge in compilation for quantum simulation is that one of the potential optimization opportunities comes from two seemingly incompatible approaches: deterministic compilation and random compilation. After the Hamiltonian is decomposed into the summation of Hamiltonian terms, the deterministic compilation will find a specific order to execute the simulation of each term and repeat this order many times to approximate the simulation of the entire Hamiltonian. The Hamiltonian terms can order for various optimization objectives, such as more gate cancellation [22, 26, 37], shorter circuit depth [37], reduced approximation error [22], circuit simplification [11, 12, 15, 66], etc. In contrast, the randomized approach will randomly sort the Hamiltonian terms [9, 51] or even randomly sample the Hamiltonian terms to assemble the final simulation circuit [8]. Theoretical analysis shows that the randomized compilation can converge asymptotically faster with lower error bounds, but the benefits from deterministic compilation are mostly lost. Previous works lie in either one of these two categories, as these two types of approaches are seemingly incompatible. To the best of our knowledge, none of them could simultaneously leverage the benefits of both approaches.

Lack of Proper Intermediate Representation: Modern classical compilers employ multiple intermediate representations (IRs) (e.g., control flow graph, static single assignment) from high-level to low-level to accommodate different optimizations. Today’s quantum compilers [3, 29, 32, 43, 56], on the other hand, are mostly built around low-level representations [13, 34, 57]. Recently, several new languages, including the Pauli IR in Paulihedral [37], the phase gadgets [11] in TKET [56], and the Hamiltonian Modeling Language in SimuQ [53], are proposed to help with compiling quantum Hamiltonian simulation. These languages capture the individual Hamiltonian terms and thus can benefit program analysis and optimization in deterministic compilation approaches. Yet, to the best of our knowledge, none of them can accommodate optimizing or tuning in the randomized compilation approaches.

Correctness Guarantee for Quantum Simulation Compilation: Generic quantum compilation optimizations, such as circuit rewriting [58], gate cancellation [47], template matching [42], and qubit mapping [46], usually execute very small-scale quantum program transformations in each step and thus can be checked by evaluating the gate matrices or formally verified (e.g., VOQC [27], Giallar [63], VyZX [35]). In contrast, compiling the quantum simulation from the input Hamiltonian to the circuit implementation is a large-scale program transformation involving many gates and qubits. Evaluating the correctness or approximation error requires calculating the exponentially large gate matrix of the entire Hamiltonian simulation circuits. Previous deterministic compilation approaches are governed by the same trotterization product formula [65]. As a result, they cannot break its approximation error bound. The randomized compilation approaches [8, 9, 51], on the other hand, rely on sophisticated ad-hoc algorithm performance analysis. The correctness guarantee for any new quantum simulation compilation involving randomization is non-trivial.

To this end, we propose MarQSim, a new framework that can advance the compilation for quantum Hamiltonian simulation programs by reconciling the deterministic and randomized compilation. An overview of MarQSim is illustrated in Fig. 1. **First**, MarQSim formulates the compilation process into sampling from a Markov chain. Sampling from a random process

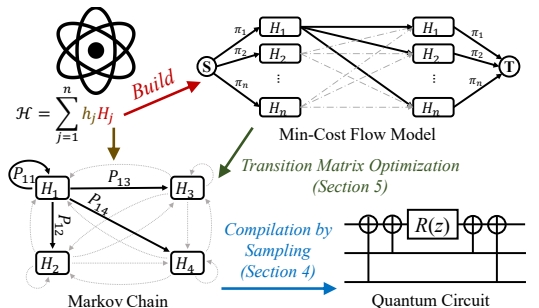


Fig. 1. Overview of MarQSim compiler framework

can naturally inherit the benefits from randomized compilation. The probability transition matrix in the Markov chain can be tuned to change the sampling tendency and thus incorporate the benefits from deterministic compilation. **Second**, MarQSim will convert an input Hamiltonian into a newly designed IR, the Hamiltonian Term Transition Graph, to encode the Hamiltonian information into a homogeneous Markov chain. The compilation process is to sample from a Markov chain whose state transition graph is our IR. As the key parameter, we rigorously prove the sufficient conditions for the Markov chain transition matrix to guarantee the overall correctness and algorithmic advantage of MarQSim compilation. **Third**, in addition to the sufficient condition, we provide a practical approach to obtain a valid and optimized transition matrix by solving a Min-Cost Flow problem. By carefully designing the flow architecture, the conditions for correctness and other optimization objectives can be intuitively encoded into the cost and capacity functions in the flow network. The solved flow can then be turned back into a transition matrix. **Finally**, we show that different optimization objectives represented by multiple transition matrices can be easily reconciled in MarQSim by a normalized weighted summation of those individual transition matrices. We also propose to evaluate the convergence speed of the sampling process by analyzing the spectra of different transition matrices. In this paper we demonstrate the combination of randomized compilation, CNOT gate cancellation, and random perturbation while extending to more optimization objectives is also possible.

The major contributions of this paper can be summarized as follows:

- (1) We propose MarQSim, a new compilation framework that can reconcile the benefits from previous deterministic and randomized compilation techniques, even if they seem incompatible, and thus opens up new optimization space for quantum simulation.
- (2) We designed a new IR, the Hamiltonian Term Transition Graph, for MarQSim to naturally formulate the compilation process into sampling from a Markov chain and a corresponding compilation algorithm. We rigorously proved the sufficient conditions to guarantee the correctness and the algorithmic advantage of MarQSim compilation.
- (3) To further incorporate more optimization objectives from deterministic compilation, we provide a Min-Cost Flow model to turn the Markov transition matrix for different ordering tendencies while the correctness conditions are enforced.
- (4) Experimental results show that MarQSim can outperform the baseline in compiling a wide range of quantum Hamiltonian simulations. The circuits generated by MarQSim contain significantly fewer gates when maintaining similar approximation accuracy.

2 PRELIMINARY

In this section, we introduce the necessary preliminary about quantum computing, quantum simulation, Markov process, and minimum-cost flow.

2.1 Qubit and Quantum State

The basic information processing unit in quantum computing is the qubit. The state of a single qubit is defined by a vector $|\psi\rangle = \alpha|0\rangle + \beta|1\rangle$ with $|\alpha|^2 + |\beta|^2 = 1$ in the two-dimensional Hilbert space spanned by the $|0\rangle$ and $|1\rangle$ basis. This representation can be perceived as the qubit simultaneous being in $|0\rangle$ and $|1\rangle$ basis with amplitude α and β , known as the superposition. After a measurement, the superposition state collapses to $|0\rangle$ or $|1\rangle$, with probability $|\alpha|^2$ and $|\beta|^2$, respectively.

To extend this idea, the N -qubit state is defined by a vector in a 2^N -dimensional Hilbert space. The basis of this Hilbert space could be constructed via the Kronecker product of N 2-dimensional Hilbert space basis as $|x_1 x_2 \dots x_N\rangle = |x_1\rangle \otimes |x_2\rangle \otimes \dots \otimes |x_N\rangle$ where $|x_i\rangle \in \{|0\rangle, |1\rangle\}$. Then, an N -qubit state can be a superposition among this basis. Once the basis is fixed, the basis's superposition coefficients form the *state vector* of a N -qubit state, which is also a vector in 2^N -dimensional Hilbert space. The rest of this paper will always use this $|0\rangle$ and $|1\rangle$ basis. Also, we can construct a multi-qubits state by combining single-qubit states using the Kronecker product in this manner $|\psi\rangle = |\psi\rangle_1 \otimes |\psi\rangle_2 \otimes \dots \otimes |\psi\rangle_N$. However, it does not entirely hold reversely. For example, the EPR pair state $(|00\rangle + |11\rangle)/\sqrt{2}$ can not be decomposed into the Kronecker product of any two single-qubit states. This phenomenon is also known as entanglement.

2.2 Quantum Program and Circuit

A quantum program (circuit) usually consists of a set of quantum gates (operators) and measurements. A quantum gate is a unitary matrix that applies to the state vector of the qubits. For example, the X gate is a single-qubit gate. Applying the X gate to a single-qubit state $\alpha|0\rangle + \beta|1\rangle$ follows matrix multiplication:

$$X = \begin{pmatrix} 0 & 1 \\ 1 & 0 \end{pmatrix} \Rightarrow X \begin{pmatrix} \alpha \\ \beta \end{pmatrix} = \begin{pmatrix} 0 & 1 \\ 1 & 0 \end{pmatrix} \begin{pmatrix} \alpha \\ \beta \end{pmatrix} = \begin{pmatrix} \beta \\ \alpha \end{pmatrix}$$

Thus, gate X transforms the state $\alpha|0\rangle + \beta|1\rangle$ to $\beta|0\rangle + \alpha|1\rangle$. A Quantum gate applied on N qubits can always be represented by a $2^N \times 2^N$ complex unitary matrix. For example, the two-qubit $CNOT$ gate has the following matrix representation:

$$CNOT = \begin{pmatrix} 1 & 0 & 0 & 0 \\ 0 & 1 & 0 & 0 \\ 0 & 0 & 0 & 1 \\ 0 & 0 & 1 & 0 \end{pmatrix}$$

In this paper, the quantum programs are represented in the quantum circuit diagram. Fig. 2 shows an example of a 3-qubit circuit. In the quantum circuit, each *horizontal line* represents a qubit. Fig 2 has three qubits: q_1 , q_2 , and q_3 . The *square blocks and \oplus symbols* on the horizontal lines represent gates applied on the qubits associated with the horizontal lines. Fig 2 has three single-qubit gates: one Y gate on q_1 , one H gate on q_3 , and a R_z gate on q_3 . Besides, a $CNOT$ gate is applied on (q_2, q_3) between the H gate and the R_z gate.

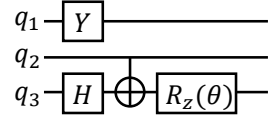


Fig. 2. Quantum circuit example

2.3 Quantum Simulation

Quantum Hamiltonian simulation involves implementing the gate $e^{i\mathcal{H}t}$ on a quantum computer where \mathcal{H} is the Hamiltonian of the simulated system. To implement the gate $e^{i\mathcal{H}t}$ with basic single- and two-qubit gates, a common practice is to decompose the Hamiltonian into a weighted sum of an array of Hamiltonian terms $\mathcal{H} = \sum_j h_j H_j$ where $h_j \in \mathbb{R}$ is the weight and H_j is the Hamiltonian term. A typical selection of H_j is the Pauli strings due to the simple implementation of $e^{i\theta_j H_j}$ ($\theta_j \in \mathbb{R}$ is a real parameter).

Pauli String: For an n -qubit system, an n -qubit Pauli string is defined as $P = \sigma_n \otimes \sigma_{n-1} \otimes \dots \otimes \sigma_1$ (or $\sigma_n \sigma_{n-1} \dots \sigma_1$ in abbreviation), where $\sigma_i \in \{I, X, Y, Z\}$ for $i \in \{1, 2, \dots, n\}$. Here, \otimes represents the Kronecker product, X , Y , and Z are Pauli operators, and I denotes the identity operator (see Appendix A.1). The operator σ_i acts on the i -th qubit.

From Pauli Strings to Circuit: A critical property of a Pauli string P is that for any $\theta \in \mathbb{R}$ the operator $\exp(iP\frac{\theta}{2})$ can be decomposed into basic gates easily. We introduce the decomposition process using an example shown in Fig. 3, which illustrates the synthesis of $\exp(iX_4Y_3Z_2I_1\frac{\theta}{2})$. First, two identical layers of single-qubit gates are added at the beginning and the end of the circuit snippet. In these two layers, the H or Y gates are applied on the qubits whose corresponding operators in the Pauli string are X (i.e., q_4) or Y (i.e., q_3), respectively. Next, one qubit whose corresponding operator in the Pauli string is not the identity is selected as the root qubit. Then, a group of CNOT gates are applied between all other qubits whose corresponding operator is not the identity and this root qubits. In this example, q_4 is the root qubit. There are CNOT gates on (q_2, q_4) and (q_3, q_4) . Then, the $R_z(\theta)$ gate is applied on the root qubit. Another group of CNOT gates is applied after the $R_z(\theta)$ gate. The CNOT gates are applied on the same qubit pairs as the first group, but the order is reversed. Note that there are other ways to generate the CNOT gate. The approach in Fig. 3 is selected to benefit from CNOT gate cancellation optimization introduced in [22].

After the $e^{i\theta_j H_j}$'s are implemented with basic gates, a compiler will further assemble them to realize e^{iHt} . We will introduce various options for this step later in Section 3.

2.4 Markov Stochastic Process

Our compiler optimization technique is based on formulating the instruction scheduling and code synthesis into a Markov stochastic process. A discrete stochastic process X is defined as an array of random variables $\{X_t \mid t \in T\}$ indexed by $t \in T = \{0, 1, 2, \dots\}$. Suppose a finite set $S = \{s_1, s_2, s_3, \dots, s_{|S|}\}$ is the state space. Each random variable X_t in the set $\{X_0, X_1, X_2, \dots\}$ takes values in a finite set $S = \{s_1, s_2, s_3, \dots, s_{|S|}\}$ known as the state space.

DEFINITION 2.1 (MARKOV CHAIN). A stochastic process X is a Markov chain if it satisfies the following condition:

$$\forall n \geq 1, \forall s, x_0, x_1, \dots, x_{n-1} \in S, \Pr[X_n = s | X_{n-1} = x_{n-1}] = \Pr[X_n = s | X_0 = x_0, \dots, X_{n-1} = x_{n-1}].$$

The probability of each random variable in a Markov chain is determined solely by the state observed in the preceding one.

DEFINITION 2.2 (HOMOGENEOUS CHAIN). A Markov chain is a homogeneous chain if it satisfies the condition:

$$\forall n \in T, \forall s_i, s_j \in S, \Pr[X_{n+1} = s_j | X_n = s_i] = \Pr[X_1 = s_j | X_0 = s_i].$$

This means the probability of transitioning from one state to another is consistent across all steps.

In the rest of this paper, all Markov chains discussed are homogeneous.

DEFINITION 2.3 (TRANSITION MATRIX). The transition matrix $\mathbf{P} = (p_{ij})$ of a homogeneous Markov chain can be defined by the transition probabilities $p_{ij} = \Pr[X_{n+1} = s_j | X_n = s_i]$ to represent the probabilities of changing among all states. It is easy to prove that for all $i, j \in \{1, 2, \dots, |S|\}$, $0 \leq p_{ij} \leq 1$ and $\sum_j p_{ij} = 1$. Naturally, the matrix $\mathbf{P}^{(n)}$ (the n -th power of matrix \mathbf{P}) where $n \in \{1, 2, 3, \dots\}$ represents the probability of changing from one state to another after exact n steps. Thus, the element of the matrix $p_{ij}^{(n)}$ is defined as $p_{ij}^{(n)} = \Pr[X_n = s_j | X_0 = s_i]$.

DEFINITION 2.4 (STATE TRANSITION GRAPH). A directed graph $G(V, E)$ can be constructed to represent a finite-state homogeneous Markov chain with a transition matrix \mathbf{P} . The vertex i in the

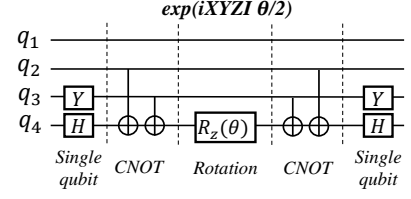


Fig. 3. Decomposition of $\exp(iX_4Y_3Z_2I_1\frac{\theta}{2})$

graph represents a state s_i for all $1 \leq i \leq |S|$ and there are $|S|$ nodes. A directed edge from state s_i to s_j exists with weight p_{ij} if $p_{ij} > 0$. Self-edges are allowed.

DEFINITION 2.5 (RECURRENT CLASS). For two vertices i and j (states s_i and s_j), if there exists a path from i to j in the constructed graph, we say that state s_i communicates with state s_j , denoted as $i \rightarrow j$. We use the notation $i \leftrightarrow j$ if states i and j can communicate with each other (i.e., $i \rightarrow j$ and $j \rightarrow i$). Note that “ \leftrightarrow ” signifies an equivalence relationship, which is reflexive, symmetric, and transitive [55]. Consequently, we can categorize all the recurrent states into recurrence classes R_1, R_2, \dots . For any two states i and j in the same recurrence class, there exists a finite integer $n \in \{0, 1, 2, \dots\}$ such that the probability of transitioning from state i to state j after exactly n steps is non-zero.

DEFINITION 2.6 (STATIONARY DISTRIBUTION). Let π denote a probability distribution of all states of a Markov chain, where π_i denotes the probability of being in state s_i . π is a stationary distribution if, provided $\Pr[X_0 = s_i] = \pi_i$ for all $i \in \{0, 1, 2, \dots\}$ at $t = 0$, the condition $\Pr[X_t = s_i] = \pi_i$ is satisfied for all time points $t \in \{1, 2, 3, \dots\}$ and states $i \in \{0, 1, 2, \dots\}$. It can be established that the distribution π is a stationary distribution if and only if it fulfills the subsequent conditions:

- (1) $\sum_i \pi_i = 1$. A stationary distribution should be normalized.
- (2) $\forall i, \pi_i = \sum_k p_{ki} \pi_k \geq 0$. A stationary distribution is not changed after one one-step state transition.

REMARK 2.1 (PROPERTIES OF STATIONARY DISTRIBUTION). Certain properties [49] of stationary distributions, which are instrumental in the proposed compiler optimization, are listed as follows:

- (1) A stationary distribution exists and is unique if there is only a single recurrence class.
- (2) If the chain possesses a unique recurrence class, then for π , the corresponding unique stationary distribution, the mixing property $\lim_{t \rightarrow \infty} p_{ij}^{(t)} = \pi_j$ holds for all i and j . As the number of steps t approaches infinity, the probability of transitioning from state i to state j after t steps converges to the corresponding entry π_j of the stationary distribution π .

All the Markov chains used in the rest of this paper are homogeneous. All their state transition graphs are strongly connected, so there is always only one recurrent class for each Markov chain. Each of the Markov chains has one unique stationary distribution. An example of such a Markov chain is in the following.

EXAMPLE 2.1. Fig. 4 shows an example of such Markov chains. On the left is the state transition graph of this chain. This Markov chain has four possible states, so this graph has four vertices. On the right is the transition matrix of this Markov chain, and the transition probabilities are also labeled as the weights on the edges of the state transition graph. It can be easily verified that for all vertices $i, j \in \{1, 2, 3, 4\}$, $i \leftrightarrow j$. Thus, there is only one recurrent class, which is $\{1, 2, 3, 4\}$. The stationary distribution of this Markov chain is unique and satisfies the conditions in Definition 2.6:

$$\begin{cases} (\pi_0 \ \pi_1 \ \pi_2 \ \pi_3) = (\pi_0 \ \pi_1 \ \pi_2 \ \pi_3) \mathbf{P} \\ \pi_0 + \pi_1 + \pi_2 + \pi_3 = 1 \end{cases} \quad (1)$$

The unique stationary distribution is:

$$\pi = (0.29 \ 0.24 \ 0.29 \ 0.18). \quad (2)$$

2.5 Minimum-Cost Flow Problem

A Minimum-Cost Flow Problem (MCFP) [68] is an optimization and decision problem to send a certain amount of flow through a flow network with the lowest cost. We first define a flow network, and an MCFP is defined upon a flow network.

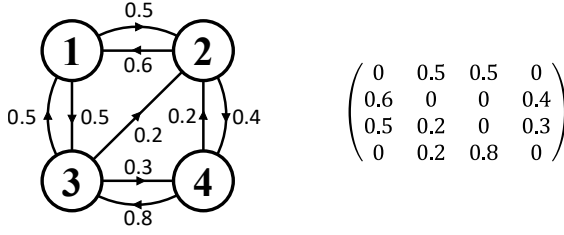


Fig. 4. A Markov chain example. Left: state transition graph. Right: state transition matrix.

DEFINITION 2.7 (FLOW NETWORK). A flow network (V, E, c, s, t) is a directed graph in which each edge possesses a capacity and receives a flow. This network, represented by a directed graph $G = (V, E)$, is assigned a non-negative capacity function $c(\cdot)$ for each edge, ensuring $c(e) > 0$ for all $e \in E$. Edges sharing the same source and target nodes are excluded. Two nodes within G are distinctly identified - one as the source s and the other as the sink t . The flow f is a function that targets the edges of the graph (commonly extended to directed edges from every pair of different nodes) and returns a real number. The flow network is subject to the following constraints:

$$\begin{cases} |f(u, v)| \leq c(u, v) \\ f(u, v) = -f(v, u) \\ \forall u \notin \{s, t\}, \sum_{v \in V} f(u, v) = 0 \end{cases} \quad (3)$$

It should be noted that $f(u, v) = f(\langle u, v \rangle)$ and $c(u, v) = c(\langle u, v \rangle)$ as is conventionally accepted. Consequently, $\sum_{v \in V} f(s, v) = \sum_{v \in V} f(v, t)$ can be verified.

DEFINITION 2.8 (MINIMUM-COST FLOW PROBLEM). In the context of MCFPs, we establish a required amount d of flow in a given flow network (V, E, c, s, t) . Then the flow f needs to satisfy

$$\begin{cases} \sum_{v \in V} f(s, v) = d \\ \sum_{v \in V} f(v, t) = d \end{cases} \quad (4)$$

MCFPs also incorporate a cost (weight) function $w(\cdot)$ for each edge. The cost associated with transporting this flow along an edge (u, v) is calculated as $f(u, v) \cdot w(u, v)$. The problem mandates a flow f of amount d to be transmitted from source s to target t . The optimization objective is to minimize the total cost of the flow across all edges:

$$\min \sum_{(u,v) \in E} w(u, v) \cdot f(u, v) \quad (5)$$

subject to all the constraints in the Equations (3) and (4) above.

EXAMPLE 2.2. Fig. 5 shows an example of a Minimum-Cost Flow Problem. This graph has 8 vertices with one source s and one sink t . On each edge, we list the weight and capacity, denoted by W and C , respectively. We set the constraint $d = 1$ in the Equation (4) and solve the minimization problem (5). The resulting network flow and cost are also listed on each edge. The red arrows show the flow's direction. The total cost of the flow is 13.2, which is the minimum cost for Equation (5) for this example. It can be easily verified that the constraints in the Equations (3) and (4) are satisfied.

3 PREVIOUS WORKS AND MOTIVATION

In this section, we introduce the previous works on optimizing the compilation of Hamiltonian simulation. We summarize the previous works in two major categories: the deterministic compilation and the randomized compilation. We briefly discuss the pros and cons of these two types of approaches and the dilemma of combining them, followed by the motivation of this work.

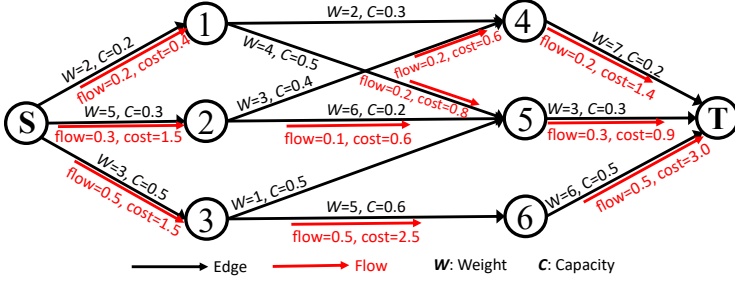


Fig. 5. An MCFP example. The minimum cost solution with flow amount 1 is obtained and the actual flow on each edge is denoted by the red arrows attached to the edges.

3.1 Deterministic Compilation with Fixed Hamiltonian Term Order

To compile the operator $e^{i\mathcal{H}t}$ into basic gates, a commonly-used approach is the Trotter-Suzuki decomposition [4, 61, 62]. Given a Hamiltonian with decomposition $\mathcal{H} = \sum_{j=1}^n h_j H_j$, the Trotter product formula [67] to approximately implement $e^{i\mathcal{H}t}$ is:

$$e^{i\mathcal{H}t} = (e^{ih_1 H_1 \Delta t} e^{ih_2 H_2 \Delta t} \dots e^{ih_n H_n \Delta t})^{\frac{t}{\Delta t}} + O(t\Delta t), \quad (6)$$

The Hamiltonian terms after decomposition should be easily implemented with basic gates. Pauli strings are a widely used decomposition basis, and the circuit implementation of a Pauli string simulation has been introduced in Section 2.3.

Note that this formula does not require any specific order of the Hamiltonian terms within one trotterization step. The first type of approach is to find a specific order for the Hamiltonian terms $\{e^{ih_1 H_1 \Delta t}, e^{ih_2 H_2 \Delta t}, \dots, e^{ih_n H_n \Delta t}\}$ with some benefits, and then repeat this fixed order $\frac{t}{\Delta t}$ times to approximate the overall Hamiltonian simulation $e^{i\mathcal{H}t}$. In this approach, the ordering of the Hamiltonian terms in the entire circuit is deterministic.

One typical benefit of Hamiltonian term ordering is gate cancellation. When the Hamiltonian terms are Pauli strings, and two consecutive terms share the same Pauli operator at some qubits, there is a potential to cancel some gates. Fig. 6 shows an example when applying the gate cancellation technique in [22]. There are two Pauli string simulation circuits for string ZZZZ and XZXZ, and they share the same Z operators on two qubits. Adding one ancillary qubit can cancel all the CNOT gates associated with these two qubits (the gates marked in rectangles in Fig. 6). To maximize the matched operators for more gate cancellation, Hastings et al. [26], Gui et al. [22], and the Paulihedral compiler [37] explored various lexical-based Hamiltonian term ordering.

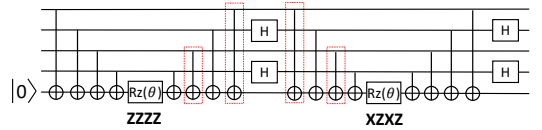


Fig. 6. CNOT gate cancellation example

Benefits beyond gate cancellation are also possible. Paulihedral compiler [37] provides another ordering option for circuit depth reduction. Some works [11, 12, 15, 66] groups the mutually commutative Pauli strings in the ordering to apply simultaneous diagonalization for circuit simplification. Gui et al. [22] also find that grouping the mutually commutative Pauli strings can reduce the trotterization error and provide better approximation.

This approach optimizes the Hamiltonian term ordering within each trotterization step and repeats one optimized order across the entire simulation circuit. Their algorithmic approximation errors are still bounded by the original product formula (Equation (6)).

3.2 Randomized Compilation with Sampling the Hamiltonian Terms

Recently, it has been observed that randomized compilation can usually yield asymptotically better performance compared with the deterministic approaches. Different from the deterministic compilation where the order of the Hamiltonian terms is fixed, the randomized compilation approaches generate the quantum circuit via random sampling from the Hamiltonian terms. Childs et al. [9] find that randomly ordering the Hamiltonian terms within each trotterization step and using different randomly generated orders across the circuit generation can provide lower approximation error. The SparSto algorithm [51] downsamples the Hamiltonian terms for each trotterization step and then randomly orders the terms within each step.

Especially, the qDrift randomized compiler [8] breaks the framework of trotterization and outperforms the deterministic compilation with an asymptotically better error bound in theory and better numerical results in practice. Given a Hamiltonian $\mathcal{H} = \sum_{j=1}^n h_j H_j$ and let $\lambda = \sum_{j=1}^n |h_j|$. The qDrift compiler will sample from an array of operators $e^{i\frac{\lambda t}{N} H_1}, e^{i\frac{\lambda t}{N} H_2}, \dots, e^{i\frac{\lambda t}{N} H_n}$ with a respective probability distribution $\frac{|h_1|}{\sum_j |h_j|}, \frac{|h_2|}{\sum_j |h_j|}, \dots, \frac{|h_n|}{\sum_j |h_j|}$ and N is the number of samples. The compiled circuit is generated by cascading the randomly sampled operators. This circuit can approximate $e^{i\mathcal{H}t}$ with an error bound $\Delta \lesssim \frac{2\lambda^2 t^2}{N}$. This algorithmic error bound can outperform the first-order trotterization (Equation (6)) in all cases and even outperform high-order trotterization most of the time in a common setup for quantum Hamiltonian simulations [8].

However, the benefits from deterministically ordering the Hamiltonian terms are lost in the randomized compilation. Because the Hamiltonian terms are randomly cascaded, there is not much control over how we can order the terms.

3.3 Comparison of the Two Types of Approaches and Our Motivation

These two types of approaches have their own pros and cons. Deterministic compilation approaches can leverage various benefits from carefully ordering the Hamiltonian terms, but the overall algorithmic approximation accuracy is not as good as that of randomized compilation. Randomized compilation benefits from better algorithmic approximation accuracy while largely losing the benefits from Hamiltonian term ordering. Naturally, to further optimize the compilation for quantum simulation, our research question is:

Can we design a compiler that can leverage the benefits of both deterministic compilation and random compilation?

Intuitively, these two types of approaches are incompatible because of their different built-in deterministic and random nature. Previously, to the best of our knowledge, it is not known how we can naturally combine these types of approaches and reconcile the benefits from both deterministic compilation and randomized compilation. This paper aims to systematically overcome this challenge and deliver a new compiler for quantum Hamiltonian simulation where the pros of both deterministic and randomized compilation can be leveraged simultaneously.

4 MARQSIM INTERMEDIATE REPRESENTATION AND COMPILATION ALGORITHM

In this section, we introduce MarQSim, a new compilation framework that can reconcile the benefits of deterministic and random compilation. As discussed above, there is a built-in contradiction between these two types of compilation approaches, and combining them requires non-trivial efforts. MarQSim tackles this challenge by starting from randomized compilation but introducing controllability in the random sampling. That is, MarQSim formulates the compilation process into sampling from a Markov stochastic process, and the controllability can be implemented by tuning the transition matrix. In the rest of this section, we will introduce a new intermediate representation

(IR), the Hamiltonian Term Transition Graph (HTT Graph), to naturally formulate and encode the Markov chain for simulating a target Hamiltonian in our MarQSim framework, followed by our compilation algorithm to convert an HTT Graph into a quantum circuit. We rigorously prove that the compilation algorithm in MarQSim can generate the correct quantum circuit without losing the algorithmic advantage of the randomized compilation for quantum simulation.

4.1 Hamiltonian Term Transition Graph as Intermediate Representation

As introduced in Definition 2.4, a state transition graph can express a homogeneous Markov chain. To formulate the compilation into sampling from such a Markov chain, MarQSim employs a new intermediate representation (IR) to encode the input Hamiltonian into the state transition graph of a Markov chain. This IR is called the Hamiltonian Term Transition Graph (HTT Graph). We first introduce how to convert an input Hamiltonian in its corresponding HTT Graph IR.

DEFINITION 4.1 (HAMILTONIAN TERM TRANSITION GRAPH (HTT GRAPH)). *Given a Hamiltonian $\mathcal{H} = \sum_{j=1}^n h_j H_j$ that is decomposed into the summation of n terms, the Hamiltonian Term Transition Graph $G_{HTT}(V, E)$ is defined as a Markov transition graph, where:*

- **Vertices:** The vertex set $V = \{v_1, v_2, \dots, v_n\}$ has n vertices to represent the n Hamiltonian terms after decomposition. There is a one-to-one correspondence between the vertices and the Hamiltonian terms. A vertex v_j represents the term H_j .
- **Edges:** A directed edge from vertex v_i to v_j exists with weight p_{ij} when $p_{ij} > 0$. Self-edges are allowed.
- **Weights:** We require that all weights p_{ij} 's satisfy $0 \leq p_{ij} \leq 1$. Especially, p_{ij} is set to be 0 when there is no edge from vertex v_i to v_j . Additionally, the summation of the weights of any vertex's outgoing edges should be 1. That is, $\sum_{1 \leq j \leq n} p_{ij} = 1$

The graph constructed by the procedure above can immediately become a state transition graph of a homogenous Markov chain. The state space of this Markov chain is the vertex set, or equivalently, the set of all Hamiltonian terms after decomposition due to the one-to-one correspondence. The transition matrix of this chain is the weights of the edges $\mathbf{P} = (p_{ij})$ as the weights are designed to satisfy the requirements of a probability transition matrix (see Definition 2.3). The weight p_{ij} on the edge from v_i to v_j represents the transition probability from the state of H_i to the state of H_j .

Fig. 7 shows an example of the HTT Graph for a Hamiltonian with four terms (H_1 to H_4) after decomposition. This graph has four vertices to represent the four Hamiltonian terms. The state space of the constructed Markov chain is $\{H_1, H_2, H_3, H_4\}$. The edges have weights to represent the corresponding state transition probability. For example, the value of p_{13} represents the probability of sampling H_3 as the next state when the current state is H_1 . The probability distribution should be normalized so we have $p_{11} + p_{12} + p_{13} + p_{14} = 1$. This means when the current state is H_1 , the summation of the probabilities for sampling all possible next states should always be 1.

How to find the transition probabilities? Note that the vertices in the HTT Graph IR have clear meanings as they are associated with the Hamiltonian terms. However, the Definition 2.3 only requires the weights of the edges to satisfy the constraints of becoming a Markov chain transition matrix. The actual values are not yet determined and will be resolved later. In the rest of this section and the next section, we will introduce the sufficient conditions of a desired transition matrix and how to optimize it, respectively.

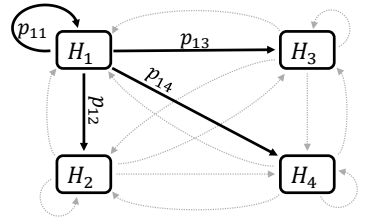


Fig. 7. HTT Graph example

Algorithm 1: Compilation As Sampling from Markov Process**Input:**

- (1) Hamiltonian $\mathcal{H} = \sum_j h_j H_j$, where H_j is a Pauli string.
- (2) Evolution time t .
- (3) Classical oracle function $Sample(p)$ that gives i with the probability of p_i from the distribution p .
- (4) Initial distribution p where $p_i = |h_i| / (\sum_j |h_j|)$.
- (5) Target precision ϵ .

Output: Quantum circuit that simulate $e^{i\mathcal{H}t}$.

```

1 Construct an HTT Graph with transition matrix  $\mathbf{P}$  for the Hamiltonian  $\mathcal{H}$ ;
  // How to obtain a transition matrix  $\mathbf{P}$  is in Section 5
2  $\lambda \leftarrow \sum_j |h_j|$ ;  $N \leftarrow \lceil \frac{2\lambda^2 t^2}{\epsilon} \rceil$ ;
3  $i \leftarrow 0$ ; // Last sampled Hamiltonian term index
4  $circuits \leftarrow \{\}$ ; // Empty quantum circuit
5 for  $n = 1 \dots N$  do
6    $i \leftarrow Sample(p)$ ;
7    $p = \mathbf{P}[i]$ ; //  $\mathbf{P}[i]$  is the  $i$ th row of  $\mathbf{P}$ 
8   Append  $e^{i\lambda t H_i / N}$  to  $circuits$ ;
9 end
10 return  $circuits$ 

```

4.2 Compiling the Hamiltonian Term Transition Graph to Quantum Circuit

By converting an input Hamiltonian into an HTT Graph, we can immediately obtain a Markov chain represented by this HTT Graph IR. The next step is to compile the HTT Graph to the quantum circuit. The compilation is implemented by sampling from the Markov chain of an HTT Graph.

The compilation algorithm in MarQSim is shown in Algorithm 1. This algorithm has several inputs, including the Hamiltonian $\mathcal{H} = \sum_j h_j H_j$ to be simulated, the desired evolution time t , a $Sample(p)$ function that can be sampled from a distribution p , an initial probability distribution obtained from the Hamiltonian decomposition, and the targeted approximation error ϵ . The output is a quantum circuit that approximates $e^{i\mathcal{H}t}$ with guaranteed approximation error below ϵ .

The first step of the compilation algorithm is to generate an HTT Graph for the Hamiltonian \mathcal{H} (by Definition 4.1). How to obtain the transition matrix \mathbf{P} will be introduced later, and we assume that we already have the matrix \mathbf{P} for now. We then need to prepare a parameter λ , which is the sum of the absolute values of the coefficients of all the Hamiltonian terms in the decomposition. We also need the number of sampling steps $N = \lceil 2\lambda^2 t^2 / \epsilon \rceil$. Finally, we will sample N steps from the Markov chain associated with the HTT graph. In the first sampling step, we sample from the set of all Hamiltonian terms $\{H_1, H_2, \dots, H_n\}$ based on the initial probability distribution p where $p_i = |h_i| / (\sum_j |h_j|)$. After the first step, the remaining $N - 1$ sampling steps are from a Markov chain where the current sampled term determines the probability distribution of sampling the next term. When the current sampled term is H_i , the probability distribution of the sampling the next term is the i -th row of the transition matrix \mathbf{P} , $[p_{i1}, p_{i2}, \dots, p_{in}]$. And p_{ij} is the probability of sampling H_j as the next term when the current term is H_i . This follows that MarQSim is formulating the compilation into sampling from a Markov chain. After a term H_i is sampled in one step, we will

append the operator $e^{i\lambda t H_i/N}$ to the final generated circuit. How to convert the $e^{i\lambda t H_i/N}$ into basic single- and two-qubit gates has been introduced earlier in Section 2.3.

Correctness of Algorithm 1: The immediate and most critical question regarding our compilation Algorithm 1 is that whether the circuit generated by Algorithm 1 can correctly approximate the quantum Hamiltonian simulation $e^{i\mathcal{H}t}$. If so, what is the error bound of the circuits sampled by Algorithm 1? The following theorem answers these questions and provides sufficient conditions that can guarantee the correctness and bounded approximation error in the final circuit generated from Algorithm 1.

THEOREM 4.1 (CORRECTNESS AND APPROXIMATION ERROR BOUND). *Given a Hamiltonian $\mathcal{H} = \sum_{j=1}^n h_j H_j$, the quantum circuit compiled by Algorithm 1 correctly approximates the operator $e^{i\mathcal{H}t}$ if the HTT graph and the corresponding transition matrix \mathbf{P} satisfies the following two conditions:*

- (1) **Strong Connectivity:** *The HTT graph is a strongly connected state transition graph, meaning that only one unique recurrence class exists, and it contains all possible states.*
- (2) **Stationary Distribution Preservation:** *The distribution $\pi_i = |h_i| / (\sum_j |h_j|)$ is stationary under the transition matrix \mathbf{P} (this is the initial distribution in our algorithm):*

$$\pi = \pi \mathbf{P} \quad \text{where} \quad \pi = \left(\frac{|h_1|}{\sum_j |h_j|} \quad \frac{|h_2|}{\sum_j |h_j|} \quad \cdots \quad \frac{|h_n|}{\sum_j |h_j|} \right)$$

The approximation error ϵ is bounded by

$$\epsilon \lesssim \frac{2\lambda^2 t^2}{N}$$

where λ is the sum of the absolute values of the Hamiltonian term coefficients, t is the simulated evolution time, and N is the number of sampling steps. (defined in Algorithm 1, line 2).

PROOF. Postponed to Appendix A.2. □

Theorem 4.1 guarantees that the quantum circuit generated by the MarQSim compilation algorithm correctly approximates the desired quantum simulation process and the error bound same as qDrift [8] once we find a transition matrix \mathbf{P} that can satisfy the sufficient conditions. Actually, the vanilla qDrift can be implemented in MarQSim with a special transition matrix.

COROLLARY 4.1 (QDRIFT IS A SPECIAL CASE IN MARQSIM). *The original qDrift algorithm [8] is a special case in our Algorithm 1, where the transition matrix \mathbf{P} is constructed directly by the desired stationary distribution. For a given Hamiltonian $\mathcal{H} = \sum_{j=1}^n h_j H_j$, qDrift can be implemented in MarQSim with the following Markov chain transition matrix:*

$$\mathbf{P} = \begin{pmatrix} \pi_1 & \pi_2 & \cdots & \pi_n \\ \pi_1 & \pi_2 & \cdots & \pi_n \\ \cdots & \cdots & \cdots & \cdots \\ \pi_1 & \pi_2 & \cdots & \pi_n \end{pmatrix} = \begin{pmatrix} \frac{|h_1|}{\sum_j |h_j|} & \frac{|h_2|}{\sum_j |h_j|} & \cdots & \frac{|h_n|}{\sum_j |h_j|} \\ \frac{|h_1|}{\sum_j |h_j|} & \frac{|h_2|}{\sum_j |h_j|} & \cdots & \frac{|h_n|}{\sum_j |h_j|} \\ \cdots & \cdots & \cdots & \cdots \\ \frac{|h_1|}{\sum_j |h_j|} & \frac{|h_2|}{\sum_j |h_j|} & \cdots & \frac{|h_n|}{\sum_j |h_j|} \end{pmatrix}$$

This transition matrix indicates that the probability to sample the next term does not depend on the previously sampled term and always selects from the stationary distribution π . It can be easily verified that this matrix satisfies the two conditions in Theorem 4.1. The fact that all $|h_j|$'s are strictly larger than 0 implies that the transition graph is a complete graph. A complete directed graph is strongly connected. $\pi = \pi \mathbf{P}$ can be checked directly.

We denote the transition matrix presented by qDrift as \mathbf{P}_{qd} . A simple numerical example of how \mathbf{P}_{qd} is constructed is provided in the following.

EXAMPLE 4.1. Consider $\mathcal{H} = 1.0 \cdot IIZZ + 0.5 \cdot IIZZ + 0.4 \cdot XXYY + 0.1 \cdot ZXZY$. In this example, $(h_1, h_2, h_3, h_4) = (1.0, 0.5, 0.4, 0.1)$. So we have the stationary distribution $(\pi_1, \pi_2, \pi_3, \pi_4) = (0.5, 0.25, 0.2, 0.05)$ and the transition matrix that implements the qDrift algorithm in our MarQSim framework is:

$$\mathbf{P}_{\text{qd}} = \begin{pmatrix} 0.5 & 0.25 & 0.2 & 0.05 \\ 0.5 & 0.25 & 0.2 & 0.05 \\ 0.5 & 0.25 & 0.2 & 0.05 \\ 0.5 & 0.25 & 0.2 & 0.05 \end{pmatrix}$$

5 COMPILER OPTIMIZATION VIA MIN-COST FLOW

In the previous section, we introduced the HTT Graph IR and the circuit compilation algorithm in the MarQSim framework, while the question of finding a transition matrix \mathbf{P} remains unsolved. We have demonstrated how to implement the baseline qDrift randomized compilation with a special transition matrix in MarQSim. However, the benefits of static Hamiltonian term ordering, such as the gate cancellation, are still not incorporated in the qDrift transition matrix. Fortunately, the MarQSim framework provides great flexibility by allowing us to tune the transition matrix for different purposes. Note that once the transition matrix satisfies the two conditions in Theorem 4.1, the overall simulation algorithmic efficiency and error bound are guaranteed. There exist many more matrices beyond the baseline qDrift transition matrix that can satisfy these two conditions. In this section, we introduce how MarQSim can find and optimize the transition matrix by formulating it in an optimization problem, the *Min-Cost Flow Problem (MCFP)*. By carefully encoding the cost and capacity functions of the edges in a flow network, MarQSim can generate transition matrices towards different Hamiltonian term ordering tendencies, and we demonstrate how to optimize for more CNOT gate cancellation by constructing a new transition matrix.

5.1 Min-Cost Flow Problem Formulation with Correctness Guarantee

We select the flow network to model our Markov chain sampling because the probability transition can be considered as probability flows that go through the vertices of the state transition graph. To model the concept of transition in the HTT graph, the overall structure of the flow network has a bipartite graph structure. A bipartite graph has two sets of vertices. Edges only exist between two vertices when they are in different sets. This can naturally represent the sampling transition from one Hamiltonian term to another Hamiltonian term.

5.1.1 Flow Network Structure from HTT Graph. In our flow network, we have two vertices set *Prev* and *Next*. Suppose there are n Hamiltonian terms in the HTT graph after decomposition. Then each of the *Prev* and *Next* sets will have n vertices to represent the n Hamiltonian terms, denoted as $Prev = \{H_i^{prev}\}$ and $Next = \{H_i^{next}\}$. $Prev = \{H_i^{prev}\}$ represents the previous sampled Hamiltonian terms. $Next = \{H_i^{next}\}$ represents the next Hamiltonian terms to be sampled. Then an edge from H_i^{prev} to H_j^{next} can represent sampling H_i in the previous step and then sampling H_j in the next step. We only allow edges from *Prev* to *Next*. A flow network also has a source vertex S and a sink vertex T . We have edges from the source vertex S to each vertex in $\{H_i^{prev}\}$ and from each vertex in $\{H_i^{next}\}$ to the sink node T . Overall, the flow goes through $S \rightarrow Prev \rightarrow Next \rightarrow T$. The graph of the constructed flow network is defined as:

$$\begin{cases} V = Prev \cup Next \cup \{S, T\} \\ E = \{ \langle H_i^{prev}, H_j^{next} \rangle | H_i^{prev} \in Prev \wedge H_j^{next} \in Next \} \cup \\ \quad \{ \langle S, H_i^{prev} \rangle | H_i^{prev} \in Prev \} \cup \\ \quad \{ \langle H_j^{next}, T \rangle | H_j^{next} \in Next \} \end{cases} \quad (7)$$

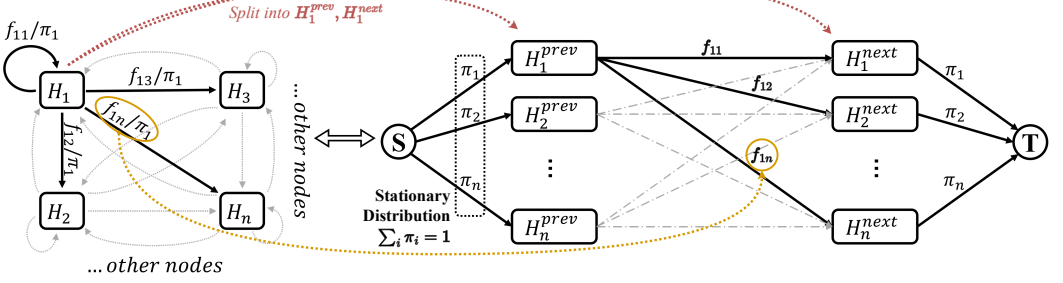


Fig. 8. Constructing the flow network from the HTT Graph. The vertex H_i in the HTT graph is converted and split into H_i^{prev} and H_i^{next} in the flow graph. The transition probability p_{ij} in the HTT graph corresponds to the flow f_{ij} from H_i^{prev} to H_j^{next} where $p_{ij} = f_{ij}/\pi_i$.

Fig. 8 shows an example of generating the structures of the flow network (on the right) based on an HTT graph (on the left). Apart from the source node and sink node, the subgraph $(\{H^{prev}\} \cup \{H^{next}\}, \langle H^{prev}, H^{next} \rangle)$ is a direct shifting of the HTT graph, where a node H_i is split into H_i^{prev} and H_i^{next} and edge $\langle H_i, H_j \rangle$ is correspondent to $\langle H_i^{prev}, H_j^{next} \rangle$.

5.1.2 From Flow to Probability Transition Matrix. After constructing the structure of the flow network, we then introduce how to generate a probability transition matrix from the flow on the edges. A flow function $f(\langle u, v \rangle)$ is attached to each edge. Consider a vertex H_i^{prev} in the *Prev* set. The only incoming flow of this vertex is the $f(\langle S, H_i^{prev} \rangle)$ from S . Its outgoing flows contain $f(\langle H_i^{prev}, H_j^{next} \rangle)$ for all H_j^{next} vertices in the *Next* set. A flow network requires that the incoming flow should be equal to the outgoing flow for all vertices except the source and sink (see the third equation in Equation (3)). So we have

$$f(\langle S, H_i^{prev} \rangle) = \sum_j f(\langle H_i^{prev}, H_j^{next} \rangle) \quad (8)$$

Similarly, we have the following for the vertex H_i^{next} in the *Next* set.:

$$f(\langle H_i^{next}, T \rangle) = \sum_j f(\langle H_j^{prev}, H_i^{next} \rangle) \quad (9)$$

When the flow network graph is constructed, the edge $\langle H_i^{prev}, H_j^{next} \rangle$ already represents sampling H_i in the previous step and then sampling H_j next and the flow in the network models the probability flow. We can use the value of

$$p_{ij} = \frac{f(\langle H_i^{prev}, H_j^{next} \rangle)}{f(\langle S, H_i^{prev} \rangle)}$$

to represent the probability of transiting from H_i to H_j and $\sum_j p_{ij} = 1$ is immediately satisfied.

From the procedure above, a probability transition matrix $\mathbf{P} = (p_{ij})$ for the HTT graph can be extracted from the flow network. We still need the transition matrix \mathbf{P} to satisfy the conditions in Theorem 4.1 to guarantee the correctness and error bound. The following theorem provides a sufficient condition that can make the transition matrix \mathbf{P} satisfy the second required condition in Theorem 4.1, the **Stationary Distribution Preservation** condition. The first required condition (strongly connected graph) will be discussed later in Section 5.3.

THEOREM 5.1 (PRESERVING STATIONARY DISTRIBUTION IN THE FLOW NETWORK). *The transition matrix \mathbf{P} extracted from a flow network mentioned above satisfies the second condition in Theorem 4.1 once the following equations hold:*

$$f(\langle S, H_i^{prev} \rangle) = f(\langle H_i^{next}, T \rangle) = \pi_i \quad (10)$$

for all $1 \leq i \leq n$.

PROOF. The general proof is in Appendix A.3. □

5.1.3 Encoding the Min-Cost Flow Problem. After constructing the flow network structure and discussing the desired probabilities of the flow, we finalize the MCFP formulation (see Section 2.5) by attaching the capacity c and cost w function onto each edge and specifying the overall required amount of flow.

Hard Constraints The hard constraints that must be satisfied to ensure a correct transition matrix have been introduced in the Theorem 5.1 above and can be naturally encoded in the capacity on the corresponding edges:

$$c(\langle S, H_i^{prev} \rangle) = c(\langle H_i^{next}, T \rangle) = \pi_i \quad (11)$$

where $\{\pi_i\}$ is the desired stationary distribution, forcing the amount of required flow to be 1. Since we have $\sum_i \pi_i = 1$, these constraints will ensure the capacity of these edges is fully utilized and then forcing the flows satisfy the requirements in Theorem 5.1.

Soft Transition Matrix Tuning The transition matrix can be tuned by changing the cost function w on the edges from $\{H_i^{prev}\}$ to $\{H_j^{next}\}$. For example, if we hope to increase the probability of sampling H_j after sampling H_i , we simply just reduce the cost on the corresponding edge $w(\langle H_i^{prev}, H_j^{next} \rangle)$ in the flow network. Then the MCFP framework will tend to increase the flow $f(\langle H_i^{prev}, H_j^{next} \rangle)$ through this edge if possible, naturally increasing the entry p_{ij} in the transition matrix and the probability of sampling H_j after H_i .

Others The cost and capacity on other edges can also be specified. In this paper, they are not used and we have the following default setup:

$$\begin{aligned} w(\langle S, H_i^{prev} \rangle) &= w(\langle H_j^{next}, T \rangle) = 0 \\ c(\langle H_i^{prev}, H_j^{next} \rangle) &= \infty \end{aligned}$$

This represents the cost function is not effective on the edges from S to $\{H_i^{prev}\}$ and those from $\{H_j^{next}\}$ to T . And we do not place capacity constraints on the edges from $\{H_i^{prev}\}$ to $\{H_j^{next}\}$.

5.2 Optimizing for CNOT Gate Cancellation

Now we illustrate how we can optimize the transition matrix for gate cancellation with the MCFP framework. To encode the gate cancellation optimization, we can let the weight function of the edge $\langle H_i^{prev}, H_j^{next} \rangle$ represent the number of gates after applying the CNOT gate cancellation between the Hamiltonian terms:

$$w(\langle H_i^{prev}, H_j^{next} \rangle) = \text{CNOT_count}(H_i^{prev}, H_j^{next})$$

The weight function $\text{CNOT_count}(H_i^{prev}, H_j^{next})$ calculates the number of CNOT gates between $R(z)$ gate of the compiled term $e^{i\lambda t H_i^{prev}/N}$ and $e^{i\lambda t H_j^{next}/N}$. In this paper, the Hamiltonian terms are Pauli strings and the gate cancellation between Pauli string simulation circuits has been widely studied in previous static Hamiltonian term ordering works (introduced in Section 3.1, Fig. 6). Here, we adopt the gate cancellation method in [22], and the weight function $\text{CNOT_count}(H_i^{prev}, H_j^{next})$

can be easily obtained based on the number of matched Pauli operators in the two Pauli strings. Given the weight function, the flow function f could be solved via an MCFP in the following:

$$\min_f \mathcal{W} = \min_f \sum_{\langle i, j \rangle \in E} f(\langle i, j \rangle) w(\langle i, j \rangle) \quad (12)$$

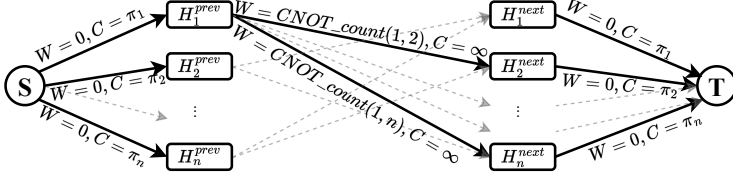


Fig. 9. Overview of the Min-Cost Flow Problem for CNOT gate cancellation

Fig. 9 shows an overview of the MCFP to optimize for CNOT gate cancellation. Each edge is annotated with a tuple of $(Weight, Capacity)$. Note that $CNOT_count(H_i^{prev}, H_i^{next}) \equiv 0$ because the two same terms can be directly combined by duplicating the time parameter without adding gates. To prevent the min-cost flow yields a trivial solution where $P_{gc} = \mathbb{I}$ (the transition matrix is the identity where all flow choose path $H_i^{prev} \rightarrow H_i^{next}$ since its cost is 0), we remove the edges of $\langle H_i^{prev}, H_i^{next} \rangle$ for all $1 \leq i \leq n$. An MCFP can be solved efficiently with various existing solvers [33]. The overall procedure of obtaining a new transition matrix via MCFP is summarized in Algorithm 2.

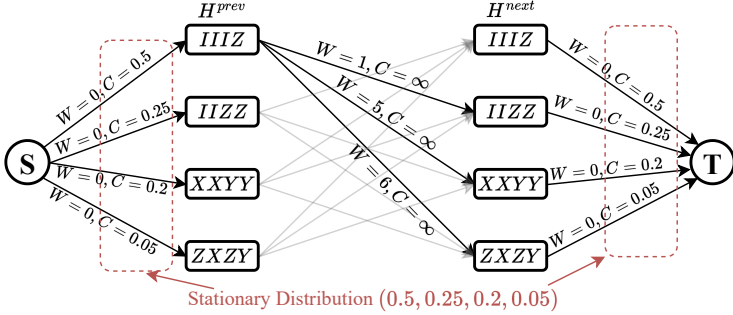


Fig. 10. Min-Cost Flow Problem to CNOT gate cancellation in Example 4.1

EXAMPLE 5.1. Consider the Hamiltonian defined in Example 4.1. Fig. 10 shows a concrete example of the MCFP formulated for optimizing the Hamiltonian in Example 4.1 (in Section 4.2). The actual cost and capacity are labeled on each edge. Solving the min-cost flow problem gives $f(\cdot)$ (for short, $f_{ij} = f(\langle H_i^{prev}, H_j^{next} \rangle)$):

$$\begin{pmatrix} f_{11} & f_{12} & f_{13} & f_{14} \\ f_{21} & f_{22} & f_{23} & f_{24} \\ f_{31} & f_{32} & f_{33} & f_{34} \\ f_{41} & f_{42} & f_{43} & f_{44} \end{pmatrix} = \begin{pmatrix} 0.0 & 0.25 & 0.2 & 0.05 \\ 0.25 & 0.0 & 0.0 & 0.0 \\ 0.2 & 0.0 & 0.0 & 0.0 \\ 0.05 & 0.0 & 0.0 & 0.0 \end{pmatrix} \quad (13)$$

Algorithm 2: Construct \mathbf{P}_{gc} out of the Min-Cost Flow Problem**Input:**

- (1) Hamiltonian $\mathcal{H} = \sum_{k=1}^n h_k H_k$.
- (2) Classic oracle function $\text{CNOT_count}(H_i, H_j) \rightarrow \mathbb{N}$.
- (3) Classic subroutine $\text{solve_mincost_flow_problem}(G, w, C) \rightarrow f$.

Output: $n \times n$ Transition Matrix \mathbf{P}_{gc}

```

1  $V \leftarrow \{S, T\}; E \leftarrow \emptyset;$ 
2 for  $i \in \{1, \dots, n\}$  do
3    $V \leftarrow V \cup \{H_i^{\text{prev}}, H_i^{\text{next}}\}; E \leftarrow E \cup \{\langle S, H_i^{\text{prev}} \rangle, \langle H_i^{\text{next}}, T \rangle\};$ 
4    $c(\langle S, H_i^{\text{prev}} \rangle) = c(\langle H_i^{\text{next}}, T \rangle) = |h_i| / (\sum_k |h_k|); w(\langle S, H_i^{\text{prev}} \rangle) = w(\langle H_i^{\text{next}}, T \rangle) = 0;$ 
5 end
6 for  $i \in \{1, \dots, n\}$  do
7   for  $j \in \{1, \dots, n\}$  do
8     if  $i \neq j$  then
9        $E \leftarrow E \cup \{\langle H_i^{\text{prev}}, H_j^{\text{next}} \rangle\};$ 
10       $c(\langle H_i^{\text{prev}}, H_j^{\text{next}} \rangle) = \infty; w(\langle H_i^{\text{prev}}, H_j^{\text{next}} \rangle) = \text{CNOT\_count}(H_i^{\text{prev}}, H_j^{\text{next}});$ 
11    end
12 end
13  $G_{\text{flow}} \leftarrow (V, E);$ 
14  $f \leftarrow \text{solve\_mincost\_flow\_problem}(G_{\text{flow}}, w, C);$ 
15 for  $i \in \{1, \dots, n\}$  do
16   for  $j \in \{1, \dots, n\}$  do
17      $\mathbf{P}_{\text{gc}ij} \leftarrow \frac{f(\langle H_i^{\text{prev}}, H_j^{\text{next}} \rangle)}{|h_i| / (\sum_k |h_k|)};$ 
18   end
19 end
20 return  $\mathbf{P}_{\text{gc}};$ 

```

The transition matrix \mathbf{P}_{gc} given by Algorithm 2, is:

$$\mathbf{P}_{\text{gc}} = \begin{pmatrix} 0.0 & 0.5 & 0.4 & 0.1 \\ 1.0 & 0.0 & 0.0 & 0.0 \\ 1.0 & 0.0 & 0.0 & 0.0 \\ 1.0 & 0.0 & 0.0 & 0.0 \end{pmatrix} \quad (14)$$

Actually, we can prove that if we compile the quantum Hamiltonian simulation circuit by executing Algorithm 1 with the transition matrix \mathbf{P}_{gc} , the expectation of the number of CNOT gates in the generated circuit is minimized and the potential from the gate cancellation (depending on the CNOT_count function) is fully utilized.

PROPOSITION 5.1 (COST IS THE EXPECTATION OF CNOT GATES COUNT). *Given the MCFP framework in Fig. 9, when the cost function $w(\langle i, j \rangle)$ in the flow network can represent the number of CNOT gates required when transiting between the Hamiltonian terms $e^{i\lambda t H_i / N}$ and $e^{i\lambda t H_j / N}$, the total cost $\mathcal{W} = \sum_{\langle i, j \rangle \in E} f(\langle i, j \rangle) w(\langle i, j \rangle)$ is the mathematical expectation number of CNOT gates between circuit snippets of H^{prev} and H^{next} if the circuit is compiled via \mathbf{P}_{gc} .*

PROOF. See Appendix A.4

□

5.3 Transition Matrix Combination

After the constraints in Theorem 5.1 are satisfied, the transition matrix generated from the MCFP has already satisfied the stationary distribution preserving condition, but the strong connectivity constraint is not guaranteed. In MarQSim, this constraint is realized by combining multiple transition matrices.

THEOREM 5.2 (COMBINING TRANSITION MATRICES). *Given an array of transition matrices $\mathbf{P}_1, \mathbf{P}_2, \dots, \mathbf{P}_k$, all of which satisfy the stationary distribution requirement ($\forall \mathbf{P}_i, \pi \mathbf{P}_i = \pi$) in Theorem 4.1, and an array of parameters $\Theta_1, \Theta_2, \dots, \Theta_k$ where $0 \leq \Theta_i \leq 1$ for all $1 \leq i \leq k$ and $\sum_{i=1}^k \Theta_i = 1$, a new transition matrix $\mathbf{P} = \sum_{i=1}^k \Theta_i \mathbf{P}_i$ also satisfies the stationary distribution requirement in Theorem 4.1.*

PROOF. $\pi \mathbf{P} = \pi \sum_{i=1}^k \Theta_i \mathbf{P}_i = \sum_{i=1}^k \Theta_i \pi \mathbf{P}_i = \sum_{i=1}^k \Theta_i \pi = \pi$ \square

Theorem 5.2 indicates that we can safely combine multiple transition matrices with normalized positive weights. This can enable reconciling multiple optimization opportunities provided by matrices together and guarantee strong connectivity.

Strong Connectivity Guarantee Recall that the transition matrix for the vanilla randomized compilation qDrift algorithm \mathbf{P}_{qd} is a valid matrix for the compilation Algorithm 1. All entries in \mathbf{P}_{qd} are strictly larger than 0 since we must have $|h_j| > 0$ in the Hamiltonian decomposition $\mathcal{H} = \sum_j h_j H_j$. For any transition matrix \mathbf{P} , we can always combine it and \mathbf{P}_{qd} by Theorem 5.2 to make the new transition matrix all positive. Then the new transition matrix will represent a complete direct graph and naturally guarantee strong connectivity. That ensures we can always find transition matrices that satisfy the two requirements to guarantee the overall correctness of the MarQSim compilation framework.

EXAMPLE 5.2. *For the Example 4.1, we can obtain a new transition matrix $\mathbf{P} = 0.4\mathbf{P}_{\text{qd}} + 0.6\mathbf{P}_{\text{gc}}$ (\mathbf{P}_{qd} and \mathbf{P}_{gc} can be found in Example 4.1 and Example 5.1, respectively) to combine the qDrift randomized compilation and the gate cancellation optimization in MarQSim. The new matrix is:*

$$\mathbf{P} = \begin{pmatrix} 0.2 & 0.4 & 0.32 & 0.08 \\ 0.8 & 0.1 & 0.08 & 0.02 \\ 0.8 & 0.1 & 0.08 & 0.02 \\ 0.8 & 0.1 & 0.08 & 0.02 \end{pmatrix} \quad (15)$$

5.4 Reasoning about Convergence Speed via Spectrum Analysis

With the transition matrix combination technique above, we can construct many transition matrices that satisfy the conditions in Theorem 4.1, and they have the same error bound. However, in practice, we observe that their actual convergence speed, indicated by the variance of the sampled circuit unitary, can still be different. In this section, we show that we can reason about the convergence speed of the sampling process by analyzing the spectrum of the transition matrix.

Usually, in a sampling process, the sampling result after the first few steps has a very large variance, and the sampling variance gradually decreases as the number of sampling steps increases. The specific sampling problem in this paper can be formulated in the following: *Suppose the initial distribution is π_0 and the transition matrix is \mathbf{P} . We are interested in how fast $\mathbf{P}^k \pi_0$ can converge to the stationary distribution π since this rate will affect the speed of our sampled Hamiltonian simulation circuit converging to the ideal circuit.*

We use the power method to reason about this convergence speed. Suppose \mathbf{P} has the following Jordan decomposition, and the eigenvalues in each Jordan block are in decreasing order:

$$\mathbf{P} = V \cdot \text{diag}(J_1, \dots, J_p) \cdot V^{-1},$$

with $|\lambda_1| > \dots > |\lambda_p|$, where J_i which is n_i dimensional Jordan matrix associate with eigenvalue λ_i .

Then we divide V according to columns, $V = (V_1, V_2, \dots, V_p)$ with $\text{rank}(V_i) = n_i$. Let $y = (y_1^T, y_2^T, \dots, y_p^T)^T = V^{-1}\pi_0$, then:

$$\mathbf{P}^k \pi_0 = \lambda_1^k [V_1 y_1 + V_2 (\frac{J_2}{\lambda_1})^k y_2 + \dots] = [V_1 y_1 + V_2 (J_2)^k y_2 + \dots], \quad (16)$$

Note that we always have $0 \leq |\lambda_i| \leq 1$, where λ_i is the spectra of a transition matrix of a Markov chain. The largest eigenvalue $\lambda_1 = 1$ is always associated with the stationary distribution π . Here $V_1 y_1$ is stationary distribution π that will remain after many sampling steps. The following terms $V_i (\frac{J_i}{\lambda_1})^k y_i$ ($1 < i \leq p$) will converge to zero, since the spectral radius: $\rho(\frac{J_i}{\lambda_1}) = |\lambda_i|/|\lambda_1| < 1$.

Equation (16) shows that the convergence speed is affected by the transition matrix's spectra distribution. Except for the large eigenvalue $\lambda_1 = 1$, more spectra with smaller values will result in a higher convergence rate. In the following example, we will investigate the spectra of the two transition matrices obtained by different methods for the same Hamiltonian.

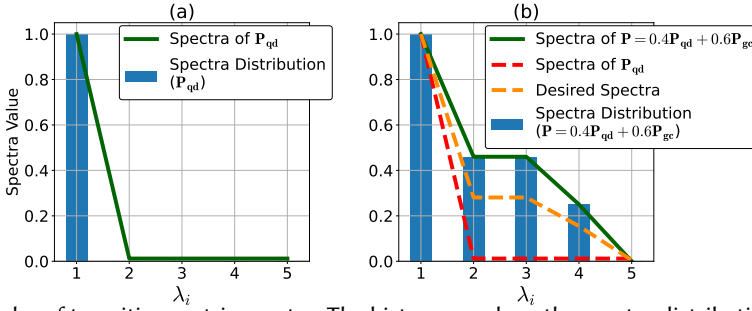


Fig. 11. Examples of transition matrix spectra. The histograms show the spectra distribution, and the lines capture the eigenvalue decreasing trend.

EXAMPLE 5.3. Given a Hamiltonian $\mathcal{H} = 1.0 \cdot \text{IIIZY} + 1.0 \cdot \text{XXIII} + 0.7 \cdot \text{ZXZYI} + 0.5 \cdot \text{IIZZXX} + 0.3 \cdot \text{XXYYZ}$. We can have two transition matrices in MarQSim to compile this Hamiltonian:

- (1) Consider the transition matrix \mathbf{P}_{qd} for vanilla qDrift (see Corollary 4.1 above). Its spectra are $\lambda_1 = 1$ and $\lambda_2 = \lambda_3 = \lambda_4 = \lambda_5 = 0$ because it has rank 1 and the only one non-zero eigenvalue is 1 corresponding to the stationary distribution. The spectra distribution of \mathbf{P}_{qd} is shown in Fig. 11 (a).
- (2) Consider the combined transition matrix $\mathbf{P} = 0.4\mathbf{P}_{\text{qd}} + 0.6\mathbf{P}_{\text{gc}}$ (\mathbf{P}_{gc} is the transition matrix optimized for CNOT gate cancellation introduced in Section 5.2.). Its spectra are $\lambda_1 = 1$, $\lambda_2 = \lambda_3 = 0.46$, $\lambda_4 = 0.25$, and $\lambda_5 = 0$. The spectra distribution of \mathbf{P} is shown in Fig. 11 (b).

To characterize the properties of the spectra, we plot the boundary of the spectra distribution to show the eigenvalue decreasing trend in Fig. 11.

The transition matrix \mathbf{P}_{qd} always has rank 1 with $\lambda_2 = \dots = \lambda_p = 0$, so it has the smallest variance in the sampled circuit unitary. In contrast, the combined transition matrix \mathbf{P} has non-zero λ_i 's for $i > 1$. Thus it has a larger variance and lower convergence speed. Such non-zero eigenvalues come from the \mathbf{P}_{gc} component. \mathbf{P}_{gc} uses these additional spectra to increase the gate cancellation.

5.5 Compilation via Random Perturbation

According to the transition matrix spectra analysis above, a desired transition matrix with faster convergence and smaller sampling variance would have a spectrum with smaller eigenvalues. That

is, its eigenvalue decreasing trend should be lower and closer to the trend of \mathbf{P}_{qd} . An example of such spectra is denoted by an orange dash in Fig. 11 (b). Our objective is to generate transition matrices with such spectra while maintaining the gate cancellation capability.

The insight of our method is that if we add some randomness in the transition matrix, the eigenvectors or the eigenspace will be changed. After combining multiple such matrices, the randomly altered eigenvectors will amortize the eigenvalues to obtain a trend with smaller eigenvalues. Meanwhile, we need to ensure that the stationary distribution eigenvector is always preserved.

Based on this insight, we proposed the following procedure to randomly perturb the transition matrix. Directly adding randomness to the transition matrix may result in invalid transition matrices that do not satisfy the requirements in Theorem 4.1. Fortunately, the randomness can be introduced in the MCFP framework without affecting the overall correctness. We can introduce a small random perturbation ϵ to the weight function in the MCFP:

$$w(\langle H_i^{\text{prev}}, H_j^{\text{next}} \rangle) \leftarrow w(\langle H_i^{\text{prev}}, H_j^{\text{next}} \rangle) + \epsilon$$

Such a randomness-adding method has two benefits:

- (1) The overall correctness is guarded by the capacity function and overall flow in the MCFP, which are not affected by the random perturbation.
- (2) The gate cancellation functionality is only slightly affected since the cost function is still close to the *gate_count*. So that we will not significantly lose the gate reduction benefits.

We can generate multiple different randomly perturbed MCFPs, solve them to obtain the transition matrices, and finally average them. The transition matrix obtained from the randomly perturbed MCFPs is denoted as \mathbf{P}_{rp} .

Finally, all the transition matrices collected in this and the previous sections, \mathbf{P}_{qd} (vanilla qDrift for strong connectivity), \mathbf{P}_{gc} (for gate cancellation), and \mathbf{P}_{rp} (for more randomness), can be combined into one new transition matrix to deliver compilation results that can not be achieved by any of them individually.

6 EVALUATION

In this section, we evaluate the performance of MarQSim. We will first introduce our experiment setup, then evaluate the performance improvement of MarQSim optimization, and finally study the compilation time consumption.

6.1 Experiment Setup

Experimental Configuration We prepared three configurations to demonstrate the effect of different transition matrices in MarQSim. **1. Baseline** is the qDrift algorithm [8] with transition matrix be $\mathbf{P} = \mathbf{P}_{\text{qd}}$ (defined in Corollary 4.1) followed by applying gate cancellation [22] on the randomized sequence. **2. MarQSim-GC** includes the transition matrix \mathbf{P}_{gc} for optimize CNOT gate cancellation with a certain weight: $\mathbf{P} = 0.4\mathbf{P}_{\text{qd}} + 0.6\mathbf{P}_{\text{gc}}$. **3. MarQSim-GC-RP** further considers adding the random perturbations, and the transition matrix is $\mathbf{P} = 0.4\mathbf{P}_{\text{qd}} + 0.3\mathbf{P}_{\text{gc}} + 0.3\mathbf{P}_{\text{rp}}$. Note that the weight perturbation ϵ increases 1 in *CNOT_count* between two Hamiltonian terms with probability 0.5 and P_{rp} are averaged from 100 different random perturbations for each benchmark.

Benchmarks We generate the Hamiltonian for various molecule or ion physical systems using the PySCF library [60] and Qiskit library [29] (including Qiskit Nature [17]). We use the Jordan Wigner fermion-to-qubit transformation [30] and the freezing core method to control the size of the Hamiltonian by only simulating the out-layer electrons. We also include the SYK models [24] from quantum field theory. The benchmark information is summarized in Table 1.

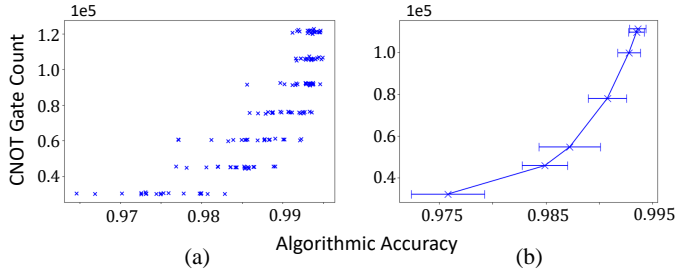
Table 1. Benchmark Information

Benchmark	Qubit#	Pauli String#	Time
Na+	8	60	$\pi/4$
Cl-	8	60	$\pi/4$
Ar	8	60	$\pi/4$
OH-	10	275	$\pi/4$
HF	10	275	$\pi/4$
LiH (froze)	10	275	$\pi/4$
BeH ₂ (froze)	12	661	$\pi/4$
LiH	12	614	$\pi/4$
H ₂ O	12	550	$\pi/4$
SYK model 1	8	210	0.15
SYK model 2	10	210	0.15
BeH ₂	14	661	0.15

Metrics We focus on the **CNOT gate count** as the optimization in our MCFP formulation. CNOT gates are usually much more expensive than single-qubit gates in the near-term noisy quantum computers [16, 20, 38]. Even in future fault-tolerant quantum computers with error correction, the overhead of CNOT gates is still considerable due to various constraints [28, 41]. We also calculate the **algorithmic accuracy**, i.e., how closely the unitary matrix U_{app} of the circuit generated by our compiler approximates the exact unitary evolution matrix $U = e^{iHt}$. This is indicated by the unitary fidelity defined as $tr(U_{app} \cdot U^\dagger)/2^n$ (n is the number of qubits). A fidelity closer to 1 is better.

Implementation We implement MarQSim in Python with Numpy. We use the Python networkx package [23] to implement and solve the MCFP. Calculating the approximated unitary in the generated circuits U_{app} is costly. We accelerate this on an NVIDIA A100 GPU with PyTorch [52] with CUDA [50]. Due to the limitation of GPU memory, we can only evaluate up to 14 qubits.

Data Processing The approximation error ϵ is set to be 0.1, 0.067, 0.05, 0.04, 0.033, 0.0286, 0.025 to make the distribution of the number of random sampling steps N relatively uniform. For each experimental configuration, we repeat the compilation 20 times as our compilation is randomized (except for the largest benchmark BeH₂, we repeat

Fig. 12. Data processing with raw data from BeH₂ (froze)

five times due to time limitation). Fig. 12 (a) shows an example of our raw data (from the BeH₂(froze) benchmark). The X-axis is the approximation fidelity. The Y-axis is the number of CNOT gates in the compiled circuit. We can roughly control the number of gates with the approximation error, and it can be observed that the data points are clustered by the number of gates. However, we can hardly know the exact approximation fidelity before we obtain the compiled quantum circuit. To ensure a fair comparison, we first take the average for each cluster and then use $y = a + e^{bx+c}$ to fit the data points. This data processing method enables us to compare the number of gates under the same simulation accuracy between 0.992 and 0.994. The interpolated data points, as well as the standard deviation of the raw data, are plotted in Fig. 12 (b).

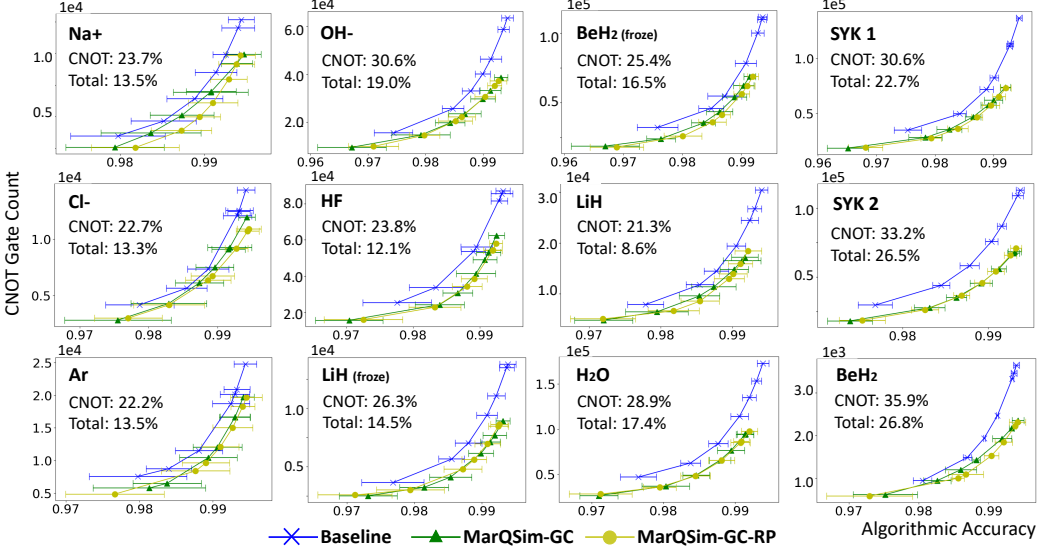


Fig. 13. Overall Improvement over all benchmarks

6.2 Overall Improvement

Fig. 13 shows the results of all the benchmarks compiled with all three configurations. We also listed the CNOT gate reduction and total gate reduction for **MarQSim-GC-RP** in each sub-figure. In summary, **MarQSim-GC** can reduce the number of CNOT gates by 25.1% on average (up to 34.6%). We also observe that **MarQSim-GC** can reduce the number of single-qubit gates by 2.1% even if the transition matrix P_{gc} is not tuned for removing single-qubit gates. The total gate reduction for **MarQSim-GC** is 14.6% on average. **MarQSim-GC-RP** can further achieve an average 27.0% reduction on CNOT gates, 5.0% reduction on single-qubit gates, and 17.0% reduction for total gates. In addition, we measure the standard deviation (σ) of the data point for each target accuracy setting. The result shows that **MarQSim-GC-RP** can reduce the standard deviation by 8.3% on average compared with the **MarQSim-GC**. This indicates that adding more randomness can make the compilation output more stable and reduce the probability of obtaining low-accuracy circuits.

6.3 Varying Transition Matrix Combination

In Section 6.2, the ratio of transition matrices (P_{qd} , P_{gc} , and P_{rp}) is fixed. In this section, we adjust the ratio combining P_{qd} and P_{gc} to understand how it affects the CNOT gate reduction. The results are shown in Fig. 14. In each subgraph, we list the CNOT gate reduction corresponding to each combination ratio. Compared with the baseline that uses only qDrift, a higher combination ratio on P_{gc} will result in higher CNOT gate reduction since the transition matrix will be more tailored for gate reduction. For the eight benchmarks, the average CNOT reduction rates are 10.3%, 23.8%, 28.0% for the transition matrix settings $P = 0.8P_{qd} + 0.2P_{gc}$, $P = 0.4P_{qd} + 0.6P_{gc}$, $P = 0.2P_{qd} + 0.8P_{gc}$ respectively. We also observe that there is an algorithmic accuracy loss as the P_{gc} component continues to increase. As discussed in Section 5.4, a larger P_{gc} component will lead to matrix spectra with larger eigenvalues, and thus the sampling will converge slower with larger variance.

6.4 Matrix Spectra Change with Random Perturbation

In this section, we investigate the impact of randomness in the transition matrix experimentally. We select the combination $P_1 = 0.4P_{qd} + 0.6P_{gc}$ and $P_2 = 0.2P_{qd} + 0.8P_{gc}$ as baseline combination

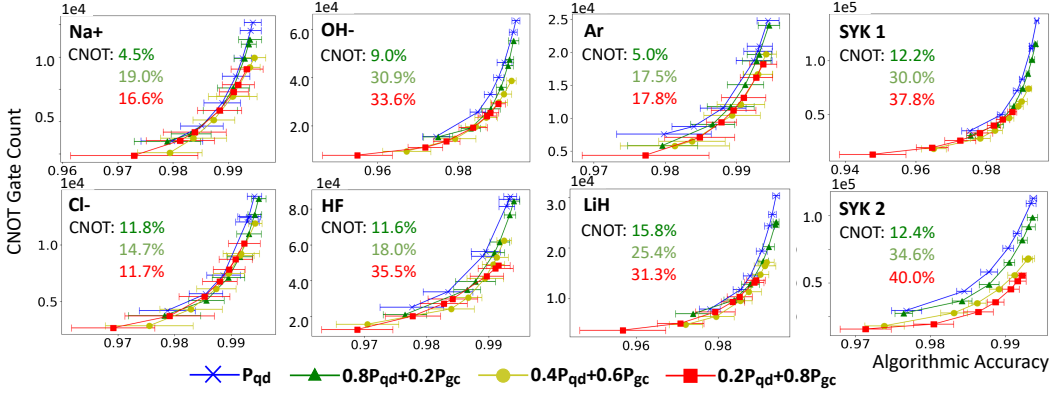


Fig. 14. Compilation results of varying (P_{qd}, P_{gc}) combination ratios

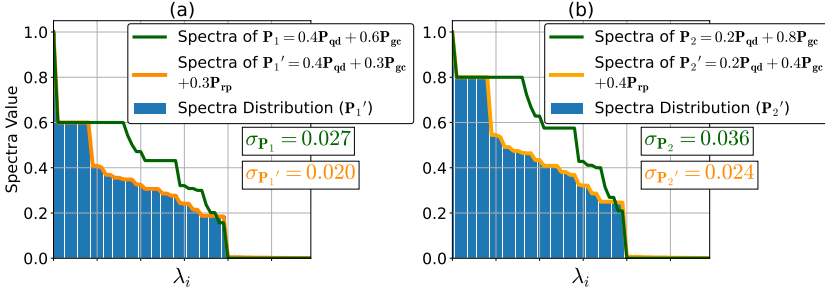


Fig. 15. Transition matrix spectra for Na+ benchmarks with different matrix combination configurations. The variance σ of the sample circuit algorithmic accuracy for each configuration is also listed.

ratios, and introduce their randomly perturbed counterparts $P'_1 = 0.4P_{qd} + 0.3P_{gc} + 0.3P_{rp}$ and $P'_2 = 0.2P_{qd} + 0.4P_{gc} + 0.4P_{rp}$, respectively. This strategy can exclude the impact of different P_{qd} component ratios.

Fig. 15 shows the spectra of the transition matrices of all these configurations for the Na+ benchmark and the trends for other benchmarks are similar. The green lines represent the eigenvalue decreasing trends of the transition matrices without perturbation, and the orange lines represent those trends for the transition matrices with random perturbation components. As discussed in Section 5.4, a transition matrix with a spectrum that has smaller eigenvalues will have faster convergence speed and smaller variance in the sampled circuits. It can be easily observed that there are significant gaps between the spectra distribution w/ and w/o the random perturbation for both configurations plotted in (a) and (b). This spectra difference leads to a substantial reduction in the standard deviation of the sampled quantum circuit. When P_{qd} contributes 0.4, the reduction of standard deviation is 26% comparing $\sigma_{P'_1}$ against σ_{P_1} . This reduction is 33% comparing $\sigma_{P'_2}$ against σ_{P_2} when P_{qd} contributes 0.2.

6.5 Impact of the Evolution Time

We also studied the impact of different evolution times. Two ions are chosen as the benchmarks: Na+ and OH- with qubit numbers equal to 8 and 10, respectively. Four evolution times are selected: $t = \frac{\pi}{6}, \frac{\pi}{3}, \frac{\pi}{2}, \frac{3\pi}{4}$. The results are shown in Fig. 16. Similarly, CNOT gate reduction and total gate reduction for MarQSim-GC-RP are also listed in each sub-figure. For MarQSim-GC, the average

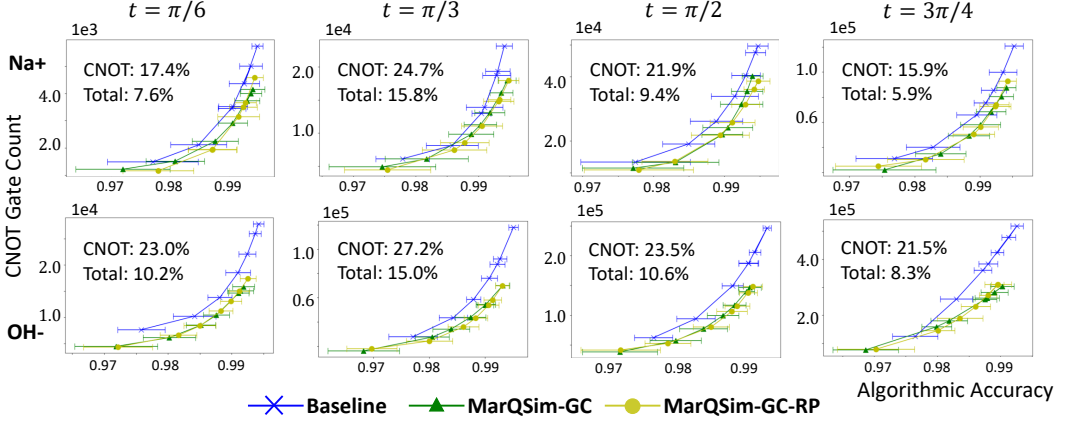


Fig. 16. Compilation optimization effect with different evolution times

Table 2. Compilation time analysis ($t = \frac{\pi}{4}$, $\epsilon = 0.05$)

Qubit#	Pauli String#	Transition Matrix Generation			Circuit Generation		
		P _{qd}	P _{gc}	P _{rp}	Baseline	MarQSim-GC	MarQSim-GC-RP
10	100	0.003	0.258	0.246	1.17	1.15	1.09
	500	0.06	22.5	23.4	78.4	75.0	76.7
	1000	0.225	169.3	168.4	585.0	584.5	580.7
20	100	0.002	0.271	0.240	1.12	1.11	1.10
	500	0.059	22.3	22.4	70.2	71.7	71.5
	1000	0.24	197.2	170.6	580.8	576.0	573.7
30	100	0.003	0.276	0.268	1.18	1.18	1.16
	500	0.06	21.9	22.2	72.1	72.3	73.3
	1000	0.232	179.4	173.8	597.3	565.0	581.1

CNOT gate reduction is 21.8%, 24.7%, 17.9%, 24.8% for $t = \frac{\pi}{6}, \frac{\pi}{3}, \frac{\pi}{2}, \frac{3\pi}{4}$ respectively. For **MarQSim-GC-RP**, the reduction is 20.2%, 25.9%, 22.7%, 18.7%. For the standard deviation, the result shows that **MarQSim-GC-RP** can reduce the standard deviation by 11.6%, 8.5%, 5.8%, -3.4% for $t = \frac{\pi}{6}, \frac{\pi}{3}, \frac{\pi}{2}, \frac{3\pi}{4}$ respectively, compared with the **MarQSim-GC**. These results confirm that the benefit of MarQSim is not affected by longer time simulation.

6.6 Compilation Time Analysis and Algorithm Complexity

In addition, we studied the scalability of MarQSim by using the randomly generated Hamiltonian at different scales. We randomly generate Hamiltonians with 10, 20, and 30 qubits. For each qubit count, the number of Hamiltonian terms (Pauli strings) is selected to be 100, 500, and 1000. We recorded the execution time to get the transition matrix and circuit, respectively. In this part, the evolution time is set to be $\frac{\pi}{4}$, and the target accuracy is set to be 0.05. The compilation time results are shown in Table 2. The entire MarQSim compilation process has two major phases. The first phase is to generate the transition matrix via MCFP. The second phase is to sample from the Markov chain to assemble the final circuit. As shown in Table 2, the compilation time mainly depends on the number of Pauli strings.

We now estimate the computational complexity for the entire MarQSim compilation flow. Suppose we have an L -qubit system with n Pauli strings, $\lambda = \sum_{i=1}^n |h_i|$ is the summation of coefficient. The evolution time is t and the target accuracy is ϵ . First, we need to get the Markov transition matrix by solving an MCFP, in which $O(n^2L)$ time is needed to calculate the weight on each edge

shown in Fig. 9, and $O(n^3 \log(n) \log(nL))$ is needed by using network simplex method solving the flow model [64]. The second step is using the transition matrix to sample the circuit. The total number of sampling steps is $N = \lceil 2\lambda^2 t^2 / \epsilon \rceil$. In each step, we need to sample from a discrete distribution of size n , which can take $\log(n)$ time [7]. Thus the overall computational complexity is $O(n^2 L + n^3 \log(n) \log(nL) + \frac{(\lambda t)^2}{\epsilon} \log(n))$. The entire compilation procedure can be accomplished in polynomial time, and the time-consuming sampling process can be easily paralleled.

7 DISCUSSION AND CONCLUSION

The compiler infrastructures co-evolve with the new applications, languages, and hardware platforms. Today’s classical computer hardware is highly sophisticated, and people usually write programs using high-level programming languages. A classical compiler employs various intermediate representations at different levels and applies corresponding program transformation/optimizations. We observe that the quantum computing area is in a transition with significant advancements in computation capability. Quantum devices with dozens or even hundreds of qubits of various technologies [10, 18, 31, 45, 59, 69] are becoming publicly available. With hardware advancements, we are able to execute programs with larger state space and more operations more reliably, which is essential for quantum advantage. Unfortunately, quantum software optimization and compilation techniques have not kept pace with hardware improvements. The low assembly-level quantum program compilation/optimizations for local gates/qubits [36, 42, 44, 46, 47, 58] have been well explored in the past decade while the high-level quantum compilation beyond the low-level gates and circuits is much less developed.

This paper aims to advance the area of high-level quantum compilation and proposes the MarQSim framework targeting the quantum Hamiltonian simulation subroutine. Even though it is not universal, the quantum Hamiltonian simulation appears in quantum programs for many purposes far beyond simulating a physical system, and thus our framework can benefit a wide range of quantum applications. More specifically, the proposed MarQSim framework reconciles the optimization opportunities from both deterministic Pauli string ordering and random sampling with new program intermediate representation and compilation optimization algorithms, exploring new program optimization design space that is, to the best of our knowledge, not reachable with previous approaches. We prove the correctness and error bound of our compilation algorithm and study the convergence speed and sampling variance via matrix spectra analysis, sharpening our understanding of the quantum simulation program compilation. We anticipate that MarQSim will continue to benefit future quantum algorithms, as quantum simulation has been a longstanding principle in algorithm design over the past few decades.

Looking forward, MarQSim is currently tuned to leverage the gate cancellation opportunities, while other optimizations in deterministic ordering may also be incorporated by combining more transition matrices. These opportunities can be grouping mutually commutative Hamiltonian terms together to reduce the approximation error [22], or even further optimized by taking the underlying hardware architecture into consideration [37]. How to find transition matrices targeting these objectives and how to further modulate the spectrum of the transition matrices remain open problems.

Moreover, the high-level optimization principle can be applied to other quantum application domains or algorithmic subroutines. There are several other significant techniques commonly used in quantum algorithm design, such as quantum phase estimation [48], amplitude amplification [6], and quantum singular value transformation [21], as well as promising application domains like machine learning [5] and optimization [1]. Developing new high-level algorithmic quantum compiler optimizations for them remains an open problem that could be addressed in future work.

REFERENCES

- [1] Amira Abbas, Andris Ambainis, Brandon Augustino, Andreas Baertschi, Harry Buhman, Carleton James Coffrin, Giorgio Cortiana, Vedran Dunjko, Daniel J. Egger, Bruce G. Elmegreen, Nicola Franco, Filippo Fratini, Bryce Fuller, Julien Gacon, Constantin Goniculea, Sander Gribling, Swati Gupta, Stuart Hadfield, Raoul Heese, Gerhard Kircher, Thomas Kleinert, Thorsten Koch, Georgios Korpas, Steve Lenk, Jakub Marecek, Vanio Markov, Guglielmo Mazzola, Stefano Mensa, Naeimeh Mohseni, Giacomo Nannicini, Corey O'Meara, Elena Peña Tapia, Sebastian Pokutta, Manuel Proissl, Patrick Reberntrost, Emre Sahin, Benjamin C. B. Symons, Sabine Tornow, Victor Valls, Stefan Woerner, Mira L. Wolf-Bauwens, Jon Yard, Sheir Yarkoni, Dirk Zechiel, Sergiy Zhuk, and Christa Zoufal. 2023. Quantum Optimization: Potential, Challenges, and the Path Forward. (12 2023). <https://doi.org/10.2172/2229681>
- [2] Daniel S. Abrams and Seth Lloyd. 1999. Quantum Algorithm Providing Exponential Speed Increase for Finding Eigenvalues and Eigenvectors. *Phys. Rev. Lett.* 83 (Dec 1999), 5162–5165. Issue 24. <https://doi.org/10.1103/PhysRevLett.83.5162>
- [3] Matthew Amy and Vlad Gheorghiu. 2020. staq—A full-stack quantum processing toolkit. *Quantum Science and Technology* 5, 3 (jun 2020), 034016. <https://doi.org/10.1088/2058-9565/ab9359>
- [4] Dominic W. Berry, Graeme Ahokas, Richard Cleve, and Barry C. Sanders. 2006. Efficient Quantum Algorithms for Simulating Sparse Hamiltonians. *Communications in Mathematical Physics* 270, 2 (Dec. 2006), 359–371. <https://doi.org/10.1007/s00220-006-0150-x>
- [5] Jacob Biamonte, Peter Wittek, Nicola Pancotti, Patrick Reberntrost, Nathan Wiebe, and Seth Lloyd. 2017. Quantum machine learning. *Nature* 549, 7671 (2017), 195–202.
- [6] G. Brassard and P. Hoyer. 1997. An exact quantum polynomial-time algorithm for Simon's problem. In *Proceedings of the Fifth Israeli Symposium on Theory of Computing and Systems*. 12–23. <https://doi.org/10.1109/ISTCS.1997.595153>
- [7] Karl Bringmann and Konstantinos Panagiotou. 2012. Efficient sampling methods for discrete distributions. In *Automata, Languages, and Programming: 39th International Colloquium, ICALP 2012, Warwick, UK, July 9-13, 2012, Proceedings, Part I* 39. Springer, 133–144.
- [8] Earl Campbell. 2019. Random compiler for fast Hamiltonian simulation. *Physical review letters* 123, 7 (2019), 070503.
- [9] Andrew M Childs, Aaron Ostrander, and Yuan Su. 2019. Faster quantum simulation by randomization. *Quantum* 3 (2019), 182.
- [10] Jerry Chow, Oliver Dial, and Jay Gambetta. 2021. IBM Quantum breaks the 100-qubit processor barrier. *IBM Research Blog* 2 (2021).
- [11] Alexander Cowtan, Silas Dilkes, Ross Duncan, Will Simmons, and Seyon Sivarajah. 2020. Phase Gadget Synthesis for Shallow Circuits. *Electronic Proceedings in Theoretical Computer Science* 318 (May 2020), 213–228. <https://doi.org/10.4204/eptcs.318.13>
- [12] Alexander Cowtan, Will Simmons, and Ross Duncan. 2020. A Generic Compilation Strategy for the Unitary Coupled Cluster Ansatz. *arXiv preprint arXiv:2007.10515* (2020).
- [13] Andrew W Cross, Lev S Bishop, John A Smolin, and Jay M Gambetta. 2017. Open quantum assembly language. *arXiv preprint arXiv:1707.03429* (2017).
- [14] Andrew J Daley, Immanuel Bloch, Christian Kokail, Stuart Flannigan, Natalie Pearson, Matthias Troyer, and Peter Zoller. 2022. Practical quantum advantage in quantum simulation. *Nature* 607, 7920 (2022), 667–676.
- [15] Arianne Meijer-van de Griend and Ross Duncan. 2020. Architecture-aware synthesis of phase polynomials for NISQ devices. *arXiv preprint arXiv:2004.06052* (2020).
- [16] Shantanu Debnath, Norbert M Linke, Caroline Figgatt, Kevin A Landsman, Kevin Wright, and Christopher Monroe. 2016. Demonstration of a small programmable quantum computer with atomic qubits. *Nature* 536, 7614 (2016), 63.
- [17] The Qiskit Nature Developers. 2023. Qiskit Nature 0.6.0. <https://doi.org/10.5281/ZENODO.7828767>
- [18] Sepehr Ebadi, Tout T. Wang, Harry Levine, Alexander Keesling, Giulia Semeghini, Ahmed Omran, Dolev Bluvstein, Rhine Samajdar, Hannes Pichler, Wen Wei Ho, Soonwon Choi, Subir Sachdev, Markus Greiner, Vladan Vuletić, and Mikhail D. Lukin. 2021. Quantum phases of matter on a 256-atom programmable quantum simulator. *Nature* 595, 7866 (01 Jul 2021), 227–232. <https://doi.org/10.1038/s41586-021-03582-4>
- [19] Richard P Feynman. 1982. Simulating physics with computers. *Int. J. Theor. Phys* 21, 6/7 (1982).
- [20] J Gambetta and S Sheldon. 2019. Cramming more power into a quantum device. *IBM Research Blog* (2019). <https://www.ibm.com/blogs/research/2019/03/power-quantum-device/>
- [21] András Gilyén, Yuan Su, Guang Hao Low, and Nathan Wiebe. 2019. Quantum singular value transformation and beyond: exponential improvements for quantum matrix arithmetics. In *Proceedings of the 51st Annual ACM SIGACT Symposium on Theory of Computing (Phoenix, AZ, USA) (STOC 2019)*. Association for Computing Machinery, New York, NY, USA, 193–204. <https://doi.org/10.1145/3313276.3316366>
- [22] Kaiwen Gui, Teague Tomesh, Pranav Gokhale, Yunong Shi, Frederic T Chong, Margaret Martonosi, and Martin Suchara. 2020. Term grouping and travelling salesperson for digital quantum simulation. *arXiv preprint arXiv:2001.05983* (2020).

- [23] Aric Hagberg, Pieter Swart, and Daniel S Chult. 2008. *Exploring network structure, dynamics, and function using NetworkX*. Technical Report. Los Alamos National Lab.(LANL), Los Alamos, NM (United States).
- [24] Stav Haldar and Anthony J Brady. 2023. A numerical study of measurement-induced phase transitions in the Sachdev-Ye-Kitaev model. *arXiv preprint arXiv:2301.05195* (2023).
- [25] Aram W. Harrow, Avinandan Hassidim, and Seth Lloyd. 2009. Quantum Algorithm for Linear Systems of Equations. *Phys. Rev. Lett.* 103 (Oct 2009), 150502. Issue 15. <https://doi.org/10.1103/PhysRevLett.103.150502>
- [26] Matthew B. Hastings, Dave Wecker, Bela Bauer, and Matthias Troyer. 2015. Improving Quantum Algorithms for Quantum Chemistry. *Quantum Info. Comput.* 15, 1–2 (jan 2015), 1–21. <https://doi.org/10.5555/2685188.2685189>
- [27] Keshu Hietala, Robert Rand, Shih-Han Hung, Xiaodi Wu, and Michael Hicks. 2021. A Verified Optimizer for Quantum Circuits. *Proc. ACM Program. Lang.* 5, POPL, Article 37 (jan 2021), 29 pages. <https://doi.org/10.1145/3434318>
- [28] Ali Javadi-Abhari, Pranav Gokhale, Adam Holmes, Diana Franklin, Kenneth R. Brown, Margaret Martonosi, and Frederic T. Chong. 2017. Optimized Surface Code Communication in Superconducting Quantum Computers. In *Proceedings of the 50th Annual IEEE/ACM International Symposium on Microarchitecture (Cambridge, Massachusetts) (MICRO-50 '17)*. Association for Computing Machinery, New York, NY, USA, 692–705. <https://doi.org/10.1145/3123939.3123949>
- [29] Ali Javadi-Abhari, Matthew Treinish, Kevin Krsulich, Christopher J Wood, Jake Lishman, Julien Gacon, Simon Martiel, Paul D Nation, Lev S Bishop, Andrew W Cross, Blake R. Johnson, and Jay M. Gambetta. 2024. Quantum computing with Qiskit. *arXiv preprint arXiv:2405.08810* (2024).
- [30] P. Jordan and E. Wigner. 1928. Über das paulische äquivalenzverbot. *Zeitschrift für Physik* 47, 9–10 (Sept. 1928), 631–651. <https://doi.org/10.1007/bf01331938>
- [31] Julian Kelly. [n. d.]. A Preview of Bristlecone, Google’s New Quantum Processor – Google Research Blog. <https://ai.googleblog.com/2018/03/a-preview-of-bristlecone-googles-new.html>. (Accessed on 07/22/2023).
- [32] N. Khammassi, I. Ashraf, J. V. Someren, R. Nane, A. M. Krol, M. A. Rol, L. Lao, K. Bertels, and C. G. Almudever. 2021. OpenQL: A Portable Quantum Programming Framework for Quantum Accelerators. *J. Emerg. Technol. Comput. Syst.* 18, 1, Article 13 (dec 2021), 24 pages. <https://doi.org/10.1145/3474222>
- [33] Zoltán Király and Péter Kovács. 2012. Efficient implementations of minimum-cost flow algorithms. *arXiv preprint arXiv:1207.6381* (2012).
- [34] Aleks Kissinger and John van de Wetering. 2020. PyZX: Large Scale Automated Diagrammatic Reasoning. *Electronic Proceedings in Theoretical Computer Science* 318 (May 2020), 229–241. <https://doi.org/10.4204/eptcs.318.14>
- [35] Adrian Lehmann, Ben Caldwell, and Robert Rand. 2022. VyZX: A Vision for Verifying the ZX Calculus. *arXiv preprint arXiv:2205.05781* (2022).
- [36] Gushu Li, Yufei Ding, and Yuan Xie. 2019. Tackling the Qubit Mapping Problem for NISQ-Era Quantum Devices. In *Proceedings of the Twenty-Fourth International Conference on Architectural Support for Programming Languages and Operating Systems (Providence, RI, USA) (ASPLOS '19)*. Association for Computing Machinery, New York, NY, USA, 1001–1014. <https://doi.org/10.1145/3297858.3304023>
- [37] Gushu Li, Anbang Wu, Yunong Shi, Ali Javadi-Abhari, Yufei Ding, and Yuan Xie. 2022. Paulihedral: A Generalized Block-Wise Compiler Optimization Framework for Quantum Simulation Kernels. In *Proceedings of the 27th ACM International Conference on Architectural Support for Programming Languages and Operating Systems (Lausanne, Switzerland) (ASPLOS '22)*. Association for Computing Machinery, New York, NY, USA, 554–569. <https://doi.org/10.1145/3503222.3507715>
- [38] Norbert M Linke, Dmitri Maslov, Martin Roetteler, Shantanu Debnath, Caroline Figgatt, Kevin A Landsman, Kenneth Wright, and Christopher Monroe. 2017. Experimental comparison of two quantum computing architectures. *Proceedings of the National Academy of Sciences* 114, 13 (2017), 3305–3310.
- [39] Seth Lloyd. 1996. Universal quantum simulators. *Science* (1996), 1073–1078.
- [40] Seth Lloyd, Masoud Mohseni, and Patrick Rebentrost. 2014. Quantum principal component analysis. *Nature Physics* 10, 9 (2014), 631–633.
- [41] Dmitri Maslov. 2016. Optimal and asymptotically optimal NCT reversible circuits by the gate types. *arXiv preprint arXiv:1602.02627* (2016).
- [42] Dmitri Maslov, Gerhard W Dueck, D Michael Miller, and Camille Negrevergne. 2008. Quantum circuit simplification and level compaction. *IEEE Transactions on Computer-Aided Design of Integrated Circuits and Systems* 27, 3 (2008), 436–444.
- [43] A. McCaskey and T. Nguyen. 2021. A MLIR Dialect for Quantum Assembly Languages. In *2021 IEEE International Conference on Quantum Computing and Engineering (QCE)*. IEEE Computer Society, Los Alamitos, CA, USA, 255–264. <https://doi.org/10.1109/QCE52317.2021.00043>
- [44] D Michael Miller and Zahra Sasanian. 2010. Lowering the quantum gate cost of reversible circuits. In *2010 53rd IEEE International Midwest Symposium on Circuits and Systems*. IEEE, 260–263.

- [45] S. A. Moses, C. H. Baldwin, M. S. Allman, R. Ancona, L. Ascarrunz, C. Barnes, J. Bartolotta, B. Bjork, P. Blanchard, M. Bohn, J. G. Bohnet, N. C. Brown, N. Q. Burdick, W. C. Burton, S. L. Campbell, J. P. Campora III au2, C. Carron, J. Chambers, J. W. Chan, Y. H. Chen, A. Chernoguzov, E. Chertkov, J. Colina, J. P. Curtis, R. Daniel, M. DeCross, D. Deen, C. Delaney, J. M. Dreiling, C. T. Ertsgaard, J. Eposito, B. Estey, M. Fabrikant, C. Figgatt, C. Foltz, M. Foss-Feig, D. Francois, J. P. Gaebler, T. M. Gatterman, C. N. Gilbreth, J. Giles, E. Glynn, A. Hall, A. M. Hankin, A. Hansen, D. Hayes, B. Higashi, I. M. Hoffman, B. Horning, J. J. Hout, R. Jacobs, J. Johansen, L. Jones, J. Karcz, T. Klein, P. Lauria, P. Lee, D. Liefer, C. Lytle, S. T. Lu, D. Lucchetti, A. Malm, M. Matheny, B. Mathewson, K. Mayer, D. B. Miller, M. Mills, B. Neyenhuis, L. Nugent, S. Olson, J. Parks, G. N. Price, Z. Price, M. Pugh, A. Ransford, A. P. Reed, C. Roman, M. Rowe, C. Ryan-Anderson, S. Sanders, J. Sedlacek, P. Shevchuk, P. Siegfried, T. Skripka, B. Spaun, R. T. Sprenkle, R. P. Stutz, M. Swallows, R. I. Tobey, A. Tran, T. Tran, E. Vogt, C. Volin, J. Walker, A. M. Zolot, and J. M. Pino. 2023. A race track trapped-ion quantum processor. *arXiv preprint arXiv:2305.03828* (2023).
- [46] Prakash Murali, Jonathan M. Baker, Ali Javadi-Abhari, Frederic T. Chong, and Margaret Martonosi. 2019. Noise-Adaptive Compiler Mappings for Noisy Intermediate-Scale Quantum Computers. In *Proceedings of the Twenty-Fourth International Conference on Architectural Support for Programming Languages and Operating Systems* (Providence, RI, USA) (ASPLOS '19). Association for Computing Machinery, New York, NY, USA, 1015–1029. <https://doi.org/10.1145/3297858.3304075>
- [47] Yunseong Nam, Neil J Ross, Yuan Su, Andrew M Childs, and Dmitri Maslov. 2018. Automated optimization of large quantum circuits with continuous parameters. *npj Quantum Information* 4, 1 (2018), 1–12.
- [48] M.A. Nielsen and I.L. Chuang. 2010. *Quantum computation and quantum information*. Cambridge university press.
- [49] James R Norris. 1998. *Markov chains*. Number 2. Cambridge university press.
- [50] NVIDIA, Péter Vingelmann, and Frank H.P. Fitzek. 2020. CUDA, release: 10.2.89. <https://developer.nvidia.com/cuda-toolkit>
- [51] Yingkai Ouyang, David R White, and Earl T Campbell. 2020. Compilation by stochastic Hamiltonian sparsification. *Quantum* 4 (2020), 235.
- [52] Adam Paszke, Sam Gross, Francisco Massa, Adam Lerer, James Bradbury, Gregory Chanan, Trevor Killeen, Zeming Lin, Natalia Gimelshein, Luca Antiga, Alban Desmaison, Andreas Kopf, Edward Yang, Zachary DeVito, Martin Raison, Alykhan Tejani, Sasank Chilamkurthy, Benoit Steiner, Lu Fang, Junjie Bai, and Soumith Chintala. 2019. PyTorch: An Imperative Style, High-Performance Deep Learning Library. In *Advances in Neural Information Processing Systems* 32. Curran Associates, Inc., 8024–8035. <http://papers.nips.cc/paper/9015-pytorch-an-imperative-style-high-performance-deep-learning-library.pdf>
- [53] Yuxiang Peng, Jacob Young, Pengyu Liu, and Xiaodi Wu. 2023. SimuQ: A Domain-Specific Language for Quantum Simulation with Analog Compilation. *arXiv preprint arXiv:2303.02775* (March 2023).
- [54] Patrick Rebentrost, Masoud Mohseni, and Seth Lloyd. 2014. Quantum Support Vector Machine for Big Data Classification. *Phys. Rev. Lett.* 113 (Sep 2014), 130503. Issue 13. <https://doi.org/10.1103/PhysRevLett.113.130503>
- [55] Howard M. Taylor Samuel Karlin. 1974. *A First Course in Stochastic Process*. ACADEMIC PRESS, INC. (LONDON) LTD., London.
- [56] Seyon Sivarajah, Silas Dilkes, Alexander Cowtan, Will Simmons, Alec Edgington, and Ross Duncan. 2020. *t|ket*: a retargetable compiler for NISQ devices. *Quantum Science and Technology* 6, 1 (nov 2020), 014003. <https://doi.org/10.1088/2058-9565/ab8e92>
- [57] Robert S Smith, Michael J Curtis, and William J Zeng. 2016. A practical quantum instruction set architecture. *arXiv preprint arXiv:1608.03355* (2016).
- [58] Mathias Soeken and Michael Kirkedal Thomsen. 2013. White Dots Do Matter: Rewriting Reversible Logic Circuits. In *Proceedings of the 5th International Conference on Reversible Computation* (Victoria, BC, Canada) (RC'13). Springer-Verlag, Berlin, Heidelberg, 196–208. https://doi.org/10.1007/978-3-642-38986-3_16
- [59] IonQ Staff. 2023. IonQ Forte: The First Software-Configurable Quantum Computer. <https://ionq.com/resources/ionq-forte-first-configurable-quantum-computer>. (Accessed on 07/22/2023).
- [60] Qiming Sun, Timothy C. Berkelbach, Nick S. Blunt, George H. Booth, Sheng Guo, Zhendong Li, Junzi Liu, James D. McClain, Elvira R. Sayfutyarova, Sandeep Sharma, Sebastian Wouters, and Garnet Kin-Lic Chan. 2018. PySCF: the Python-based simulations of chemistry framework. *WIREs Computational Molecular Science* 8, 1 (2018), e1340. <https://doi.org/10.1002/wcms.1340> arXiv:<https://wires.onlinelibrary.wiley.com/doi/pdf/10.1002/wcms.1340>
- [61] Masuo Suzuki. 1990. Fractal decomposition of exponential operators with applications to many-body theories and Monte Carlo simulations. *Physics Letters A* 146, 6 (1990), 319 – 323. [https://doi.org/10.1016/0375-9601\(90\)90962-N](https://doi.org/10.1016/0375-9601(90)90962-N)
- [62] Masuo Suzuki. 1991. General theory of fractal path integrals with applications to many-body theories and statistical physics. *J. Math. Phys.* 32, 2 (Feb. 1991), 400–407. <https://doi.org/10.1063/1.529425>
- [63] Runzhou Tao, Yunong Shi, Jianan Yao, Xupeng Li, Ali Javadi-Abhari, Andrew W. Cross, Frederic T. Chong, and Ronghui Gu. 2022. Giallar: Push-Button Verification for the Qiskit Quantum Compiler. In *Proceedings of the 43rd ACM SIGPLAN International Conference on Programming Language Design and Implementation* (San Diego, CA, USA) (PLDI 2022). Association for Computing Machinery, New York, NY, USA, 641–656. <https://doi.org/10.1145/3519939.3523431>

- [64] Robert E Tarjan. 1997. Dynamic trees as search trees via euler tours, applied to the network simplex algorithm. *Mathematical Programming* 78, 2 (1997), 169–177.
- [65] Hale F Trotter. 1959. On the product of semi-groups of operators. *Proc. Amer. Math. Soc.* 10, 4 (1959), 545–551.
- [66] Ewout Van Den Berg and Kristan Temme. 2020. Circuit optimization of Hamiltonian simulation by simultaneous diagonalization of Pauli clusters. *Quantum* 4 (2020), 322.
- [67] James D. Whitfield, Jacob Biamonte, and Alán Aspuru-Guzik. 2011. Simulation of electronic structure Hamiltonians using quantum computers. *Molecular Physics* 109, 5 (mar 2011), 735–750. <https://doi.org/10.1080/00268976.2011.552441>
- [68] Wikipedia contributors. 2023. Minimum-cost flow problem — Wikipedia, The Free Encyclopedia. https://en.wikipedia.org/w/index.php?title=Minimum-cost_flow_problem&oldid=1184915760 [Online; accessed 16-November-2023].
- [69] Jonathan Wurtz, Alexei Bylinskii, Boris Braverman, Jesse Amato-Grill, Sergio H. Cantu, Florian Huber, Alexander Lukin, Fangli Liu, Phillip Weinberg, John Long, Sheng-Tao Wang, Nathan Gemelke, and Alexander Keesling. 2023. Aquila: QuEra’s 256-qubit neutral-atom quantum computer. *arXiv preprint arXiv:2306.11727* (2023).

A APPENDIX

A.1 Pauli Matrices

The identity gate I is the identity matrix \mathbb{I} . The matrix representation of the Pauli matrices is:

$$X = \begin{pmatrix} 0 & 1 \\ 1 & 0 \end{pmatrix} \quad Y = \begin{pmatrix} 0 & -i \\ i & 0 \end{pmatrix} \quad Z = \begin{pmatrix} 1 & 0 \\ 0 & -1 \end{pmatrix}$$

A.2 Proof of Theorem 4.1

[Correctness and Approximation Error Bound] Given a Hamiltonian $\mathcal{H} = \sum_{j=1}^n h_j H_j$, the quantum circuit compiled by Algorithm 1 correctly approximates the operator $e^{i\mathcal{H}t}$ if the HTT graph and the corresponding transition matrix \mathbf{P} satisfies the following two conditions:

- (1) **Strong Connectivity:** The HTT graph is a strongly connected state transition graph, meaning that only one unique recurrence class containing all possible states exists.
- (2) **Stationary Distribution Preservation:** The distribution $\pi_i = |h_i| / (\sum_j |h_j|)$ is stationary under the transition matrix \mathbf{P} (this is the initial distribution in our algorithm):

$$\pi = \pi \mathbf{P} \quad \text{where} \quad \pi = \left(\frac{|h_1|}{\sum_j |h_j|} \quad \frac{|h_2|}{\sum_j |h_j|} \quad \cdots \quad \frac{|h_n|}{\sum_j |h_j|} \right)$$

The approximation error ϵ is bounded by $\epsilon \lesssim 2\lambda^2 t^2 / N$, where λ is the sum of the absolute values of the Hamiltonian term coefficients, t is the simulated evolution time, and N is the number of sampling steps. (defined in Algorithm 1, line 2).

PROOF. The first condition asserts the stationary distribution mentioned in condition (2) is unique, and every Hamiltonian can be reached for a given initial state. This can be proved by contradiction. Suppose the HTT graph is not strongly connected. Then there exists at least one pair of vertices v_i and v_j where we can not reach v_j from v_i . It is possible that we sample the term H_i in the first step and then the term H_j cannot be included in the entire sampling process. This will change the overall Hamiltonian we are simulating and lead to wrong results. By contradiction, the HTT graph needs to be strongly connected.

Next, we construct the evolution channel for every step according to our transition matrix. We denote $\tau = \lambda t / N$. For step i , the evolution channel can be constructed as:

$$\mathcal{E}_i(\rho) = \sum_{j=1}^n p_j^{(i)} e^{i\tau H_j} \rho e^{-i\tau H_j}$$

where $p_j^{(i)}$ stands for the probability of getting the Hamiltonian term H_j in the i -th sampling step.

Note that our initial state probability $p^{(1)}$ in Algorithm 1 is exactly the stationary distribution π of transition matrix, thus $p^{(i)} = (p_1^{(i)}, p_2^{(i)}, \dots, p_n^{(i)})$ can be calculated recurrently:

$$p^{(i)} = p^{(i-1)} \mathbf{P} = \dots = p^{(1)} \mathbf{P}^{i-1} = \pi$$

indicates the evolution channel in each step is identical:

$$\mathcal{E}_i(\rho) = \sum_{j=1}^n p_j^{(i)} e^{i\tau H_j} \rho e^{-i\tau H_j} = \sum_{j=1}^n p_j e^{i\tau H_j} \rho e^{-i\tau H_j} = \mathcal{E}(\rho)$$

Using Taylor series expansions and $p_j = h_j / \lambda$, we have that to leading order in τ ,

$$\mathcal{E}(\rho) = \rho + i \sum_j \frac{h_j \tau}{\lambda} (H_j \rho - \rho H_j) + O(\tau^2).$$

Consider the channel \mathcal{U}_N , which is $\frac{1}{N}$ of the full dynamics of the Hamiltonian simulation:

$$\begin{aligned}\mathcal{U}_N(\rho) &= e^{itH/N} \rho e^{-itH/N} \\ &= \rho + i \frac{t}{N} (H\rho - \rho H) + O\left(\frac{t^2}{N^2}\right),\end{aligned}$$

where we have expanded out to the leading order in t/N . Using $H = \sum_j h_j H_j$, we find:

$$\mathcal{U}_N(\rho) = \rho + i \sum_j^L \frac{th_j}{N} (H_j \rho - \rho H_j) + O\left(\frac{t^2}{N^2}\right).$$

Comparing \mathcal{E} and \mathcal{U}_N , we see that the zeroth and first-order terms match. The higher-order terms typically do not match, and a more rigorous analysis (see [8] for the details) shows that the channels \mathcal{E} and \mathcal{U}_N differ by an amount bounded by

$$\delta \leq \frac{2\lambda^2 t^2}{N^2} e^{2\lambda t/N} \approx \frac{2\lambda^2 t^2}{N^2}.$$

Thus the error Δ of N repetitions $\mathcal{E}_1 \mathcal{E}_2 \cdots \mathcal{E}_N = \mathcal{E}^N$ relative to the target unitary U is

$$\Delta = N\delta \lesssim \frac{2\lambda^2 t^2}{N}.$$

□

A.3 Proof of Theorem 5.1

[Preserving Stationary Distribution in the Flow Network] The transition matrix \mathbf{P}_1 extracted from a flow network mentioned above satisfies the second condition in Theorem 4.1 once the following equations hold:

$$f(\langle S, H_i^{prev} \rangle) = f(\langle H_i^{next}, T \rangle) = \pi_i$$

for all $1 \leq i \leq n$.

PROOF. Given $\pi = (\pi_1, \pi_2, \dots, \pi_n)$ defined in Theorem 4.1, the product of π and the transition matrix \mathbf{P} can be calculated as:

$$\begin{aligned}(\pi \mathbf{P})(i) &= \sum_j \pi_j \mathbf{P}(j, i) \\ &= \sum_j \pi_j \frac{f(\langle H_j^{prev}, H_i^{next} \rangle)}{f(\langle S, H_j^{prev} \rangle)} \\ &= \sum_j f(\langle H_j^{prev}, H_i^{next} \rangle) \\ &= f(\langle H_i^{next}, T \rangle) \\ &= \pi_i\end{aligned}$$

which indicates that π is the stationary distribution of \mathbf{P} .

A special case is that there exists i , s.t. $\pi_i > 0.5$. In this case, a flow satisfies Equation (10) does not exist. This issue can be mitigated by further decomposing H into $\sum_{j \neq i} h_j H_j + 0.5 \cdot h_i H_i + 0.5 \cdot h_i H_i$. Then there exists no $\pi_i > 0.5$.

□

A.4 Proof of Proposition 5.1

[Cost is the Expectation of CNOT Gate Count] Given the MCFP framework in Fig. 9, when the cost function $w(\langle i, j \rangle)$ in the flow network can represent the number of CNOT gates required when transiting between the Hamiltonian terms $e^{i\lambda t H_i/N}$ and $e^{i\lambda t H_j/N}$, the total cost $\mathcal{W} = \sum_{\langle i, j \rangle \in E} f(\langle i, j \rangle) w(\langle i, j \rangle)$ is the mathematical expectation number of CNOT gates between circuit snippets of H^{prev} and H^{next} if the circuit is compiled via \mathbf{P}_{gc} .

PROOF. We denote the random variable $\#G$ as the CNOT gate count between H^{prev} and H^{next} . To calculate the expectation, we could decompose into each case $\#G_{ij}$ of the transition (sampling) from H_i^{prev} to H_j^{next} . Note that, based on the definition, there is always $\#G_{ij} = \text{CNOT_count}(H_i^{prev}, H_j^{next})$.

$$\begin{aligned}
\mathbb{E}[\#G] &= \sum_j \Pr[H^{prev} = H_i^{prev}] \cdot \mathbb{E}[\#G_{ij} | H^{prev} = H_i^{prev}] \\
&= \sum_i \pi_i \sum_j \Pr[H^{next} = H_j^{next} | H^{prev} = H_i^{prev}] \cdot \text{CNOT_count}(H_i^{prev}, H_j^{next}) \\
&= \sum_i \pi_i \cdot \sum_j \mathbf{P}_{gc_{ij}} \cdot \text{CNOT_count}(H_i^{prev}, H_j^{next}) \\
&= \sum_i \sum_j f(\langle H_i^{prev}, H_j^{next} \rangle) \cdot \text{CNOT_count}(H_i^{prev}, H_j^{next}) \\
&= \sum_i \sum_j f(\langle H_i^{prev}, H_j^{next} \rangle) \cdot w(H_i^{prev}, H_j^{next}) \\
&= \sum_{\langle i, j \rangle \in E} f(\langle i, j \rangle) \cdot w(\langle i, j \rangle) \tag{17}
\end{aligned}$$

The last step holds since the cost defined for edges $\langle S, H^{prev} \rangle$ and $\langle H^{next}, T \rangle$ is 0. \square